2023 S.T. Yau High School Science Award (Asia)

Research Report

The Team

Registration Number: **Phy-186**

Name of team member: LEONG POK HEI
School: PUI CHING MIDDLE SCHOOL, MACAU
Country: MACAU, CHINA

Name of supervising teacher: LEONG PUI CHAN
Job Title: Physics Teacher
School: PUI CHING MIDDLE SCHOOL, MACAU
Country: MACAU, CHINA

Title of Research Report

Complex dynamical behavior and stochastic resonance phenomena of a nonlinear pendulum

Date

14 August 2023

Complex dynamical behavior and stochastic resonance phenomena of a nonlinear pendulum

LEONG POK HEI

Abstract

In this thesis, we use a nonlinear pendulum experiment to analyze the nonlinear dynamical behavior of the pendulum under the action of constant torque, periodic torque, and random torque simultaneously. We use both qualitative and quantitative methods to analysis the nonlinear physics of the pendulum and find the corresponding relationship between the modes of motion of the pendulum and the form of the external torques. We describe the model as a dynamical system, find out the fixed points and calculate the bifurcation curves by Melnikov's method and the Average Theorem. We also derive the curve of the angular position versus angular velocity in phase space. The solution gives both the qualitative and quantitative understanding of the complex dynamics in phase space.

We also investigate the effect of random torque on the pendulum. We model the random torque as a white noise signal, we add a white noise term to the model. The noise is described by a random process. The cooperative effect of noise and applied periodic torque can excite the system and induce the so-called Stochastic Resonance. We calculate the autocorrelation function and power spectrum by numerical method and also by perturbation. We compare the above with the noiseless case. We analysis the power spectrum and found the condition of stochastic resonance.

Keywords: Fixed points, bifurcation curves, white noise, autocorrelation function, stochastic resonance, power spectrum

Acknowledgement

The author would like to thank my physics teacher, LEONG PUI CHAN for his guidance on this paper and for contributions to the construction of the experiment equipment.

Commitments on Academic Honesty and Integrity

We hereby declare that we

1. are fully committed to the principle of honesty, integrity and fair play throughout the competition.
2. actually perform the research work ourselves and thus truly understand the content of the work.
3. observe the common standard of academic integrity adopted by most journals and degree theses.
4. have declared all the assistance and contribution we have received from any personnel, agency, institution, etc. for the research work.
5. undertake to avoid getting in touch with assessment panel members in a way that may lead to direct or indirect conflict of interest.
6. undertake to avoid any interaction with assessment panel members that would undermine the neutrality of the panel member and fairness of the assessment process.
7. observe the safety regulations of the laboratory(ies) where the we conduct the experiment(s), if applicable.
8. observe all rules and regulations of the competition.
9. agree that the decision of YHSA(Asia) is final in all matters related to the competition.

We understand and agree that failure to honour the above commitments may lead to disqualification from the competition and/or removal of reward, if applicable; that any unethical deeds, if found, will be disclosed to the school principal of team member(s) and relevant parties if deemed necessary; and that the decision of YHSA(Asia) is final and no appeal will be accepted.

(Signatures of full team below)

梁博晞

Name of team member: LEONG POK HEI

梁沛津

Name of supervising teacher: LEONG PUI CHAN

Noted and endorsed by

PUI CHING MIDDLE SCHOOL 澳門 培正中學 MACAU

(signature)

Name of school principal: Kou Kam fai

Table of Contents

Chapter 1 Introduction

This paper studies the dynamics of a nonlinear pendulum under the action of external torques. We use Melnikov's method and Average Theorem [1] to calculate the bifurcation curves of the nonlinear pendulum under the action of fixed torque and periodic torque respectively. In general, when the strength of external torque is increased, the angular velocity of the pendulum is also increased, however, we use the nonlinear mathematical method to find that the angular velocity of the pendulum will be kept constant under certain conditions, i.e., steps appear on the graph of angular velocity versus torque. In addition, when the external torque decreases, the angular velocity of the pendulum also appears hysteresis under certain conditions. On the basis of the periodic motion of the pendulum, we add a random external torque to the system, and it can be regarded as the vibration under the interference of white noise. We found that under certain conditions, the amplitude of the pendulum will be enhanced under the influence of white noise, the white noise has a positive feedback effect on the pendulum motion, the effect of the weak signal on the pendulum is amplified, which is the so-called stochastic resonance phenomenon [12], [13].

The experimental equipment in this paper, we use the nonlinear pendulum in the PASCO chaos experiment [8], [9], [10]. We study the motion of a mass installed on the rotating disk, we treat the disk and the mass as a system and observe the motion under the action of external torques. We Use sensors mounted on the system to investigate the modes of vibration of the pendulum. We study the physics of the nonlinear pendulum under the influence of external torques, and derive the equation of motion of the pendulum. We use the software “ORIGIN” to stimulate the motion of the pendulum, and analysis the nonlinear physics of the pendulum qualitatively. Since the equation of motion is nonlinear, we find that the motion of the pendulum is complex and sensitive to the applied torques and initial conditions [9], [10].

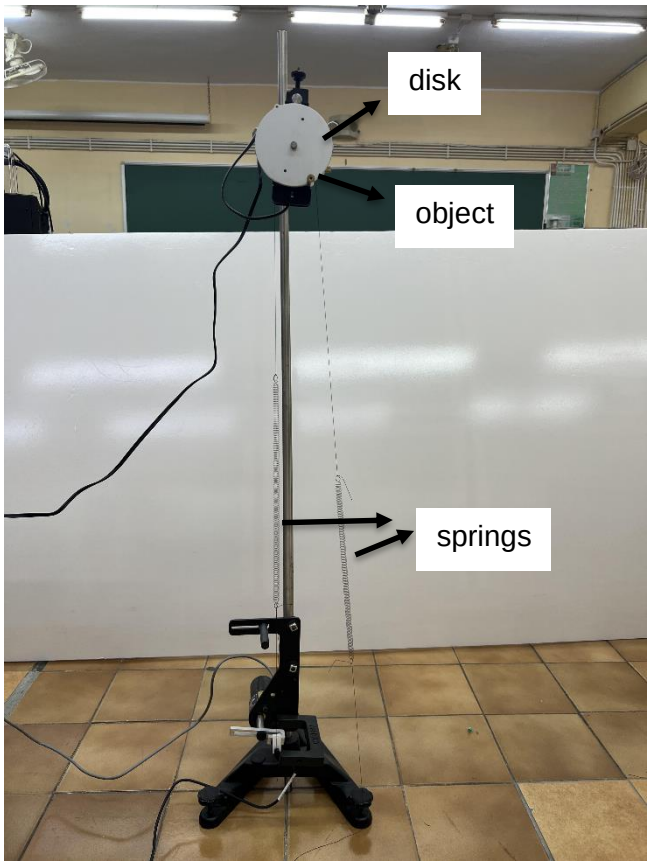

Fig. 1

The nonlinear pendulum is shown in figure 1, the mass of the disk is M and the mass of the object installed on the edge of the disk is m, as shown in figure 2. The moment of inertia of the system is $I = I_{disk} + I_{object} = \frac{1}{2}MR^2 + mL^2,$ where *R* is the radius of the disk and *L* is the distance of the object from the center of the disk.

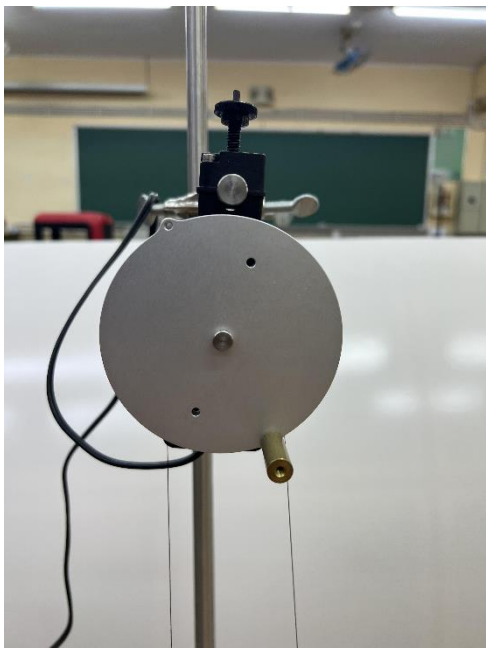

Fig. 2

When the angular displacement of the object is ϕ from the equilibrium position, the gravitational torque acts on the object is

$$T_G = mgL\sin\phi \tag{1.1}$$

As shown in Fig. 3

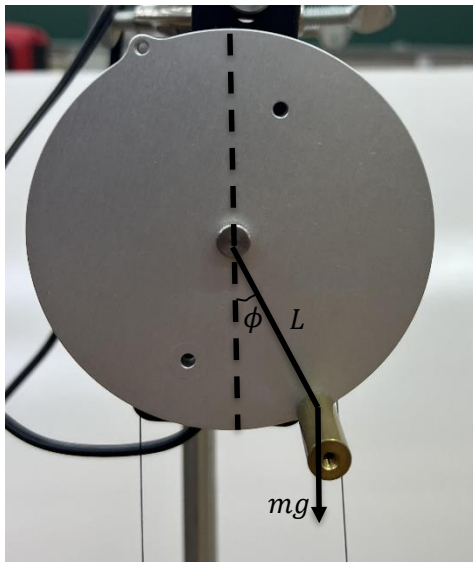

Fig. 3

The external periodic driving torque acts on the disk is $T_{ext} = T_{max}\sin(\omega t + \theta_0)$, where T_{max} is the amplitude and ω is the angular frequency of the torque respectively, θ_0 is the initial phase of the object, which can be adjusted by the tension of the spring initially. Using Hooke's law, T_{max} can be written as $T_{max} = F_{max}R = kAR$, where k is the effective spring constant, A is the amplitude of the driving force and R is the radius of the disk, it is the moment arm of the external torque.

The external periodic driving torque is

$$T_{ext} = kAR\sin(\omega t + \theta_0) \tag{1.2}$$

Also there is a constant torque T_0 acts on the disk. From Newton's second law:

$$T = I\alpha \tag{1.3}$$

Substituting (1.1), (1.2) into (1.3),

$$T_{ext} + T_0 - T_G - T_f = I\alpha$$

where $T_f = \gamma\dot{\phi}$ is the resistance torque and $\alpha = \ddot{\phi}$ is the angular acceleration of the object.

The equation of motion of the object is:

$$kAR\sin(\omega t+\theta_0)+T_0-mgL\sin\phi-\gamma\dot{\phi}\ =I\ddot{\phi} \tag{1.4}$$

From (1.4), we have

$$\begin{gathered} I\ddot{\phi}\ +\gamma\dot{\phi}\ +mgL\sin\phi=T_0+kAR\sin(\omega t+\theta_0)\\ \ddot{\phi}\ +\left(\frac{\gamma}{I}\right)\dot{\phi}+\left(\frac{mgL}{I}\right)\sin\phi=\frac{T_0}{I}+\left(\frac{kAR}{I}\right)\sin(\omega t+\theta_0)\end{gathered} \tag{1.5}$$

(1.5) is the equation of motion of the object attached on the rotating disk. From (1.5), we know that this is a nonlinear equation. It will exhibit complex and chaotic behavior under certain conditions [10], [13].

In the following chapters, we will use the method of nonlinear physics to solve (1.5) and investigate the dynamics of the nonlinear pendulum under certain conditions. we also use numerical analysis to explore the physics of the system under fixed external torque, periodic external torque and random torque respectively.

Chapter 2 Complex dynamics of a nonlinear pendulum

2.1 A transformation of the motion of pendulum in the absence of noise

The equation of motion

$$I\ddot{\phi} + \gamma\dot{\phi} + mgL\sin\phi = T_0 + T_{ext} \tag{2.1}$$

Where $T_{ext} = kAR\sin(\omega t + \theta_0)$

Hence the equation of motion of the pendulum is:

$$I\ddot{\phi} + \gamma\dot{\phi} + mgL\sin\phi = T_0 + kAR\sin(\omega t + \theta_0) \tag{2.2}$$

Let $\tau = \omega_0 t$, where $\omega_0 = \sqrt{\frac{mgL}{I}}$ and $\rho = \frac{T_0}{mgL}$, $\alpha = \frac{kAR}{mgL}$, we have

$$\dot{\phi} = \frac{d\phi}{dt} = \frac{d\phi}{d\tau}\cdot\frac{d\tau}{dt} = \omega_0\frac{d\phi}{d\tau}$$

$$\ddot{\phi} = \frac{d}{dt}\left(\frac{d\phi}{dt}\right) = \frac{d}{d\tau}\left(\omega_0\frac{d\phi}{d\tau}\right)\frac{d\tau}{dt} = {\omega_0}^2\frac{d^2\phi}{d\tau^2}$$

$\omega t = \omega\cdot\frac{\tau}{\omega_0} = \left(\frac{\omega}{\omega_0}\right)\tau = \Omega\tau$, where $\Omega = \frac{\omega}{\omega_0}$

From the above transformation, the equation of motion of the pendulum is:

$$\frac{d^2\phi}{d\tau^2} + \frac{1}{\sqrt{\beta}}\frac{d\phi}{d\tau} + \sin\phi = \rho + \alpha\sin(\Omega\tau + \theta_0) \tag{2.3}$$

where $\beta = \frac{ImgL}{\gamma}$

Here we set $\theta_0 = 0$ without loss of integrity, we investigate the equation of motion of the object mounted on the disk:

$$\frac{d^2\phi}{d\tau^2} + \frac{1}{\sqrt{\beta}}\frac{d\phi}{d\tau} + \sin\phi = \rho + \alpha\sin\Omega\tau \tag{2.4}$$

2.2 Autonomous case

2.2.1 dynamical system

The equation governing the behavior of the pendulum in the autonomous case can be written as

$$\frac{d^2\phi}{d\tau^2} + \frac{1}{\sqrt{\beta}}\frac{d\phi}{d\tau} + \sin\phi = \rho \tag{2.5}$$

It can be further revised as [3], [6]

$$\begin{cases} \dfrac{d\phi}{d\tau} = y, \\ \dfrac{dy}{d\tau} = \rho - \dfrac{y}{\sqrt{\beta}} - \sin\phi \end{cases} \tag{2.6}$$

It is known that any solution of (2.6) can be written in the form [4]

$$\frac{d\phi^*(\tau, \phi_0, y_0, \tau_0)}{d\tau} = y_{tr}(\tau, \phi_0, y_0, \tau_0) + y^*(\tau, \phi_0, y_0, \tau_0) \tag{2.7}$$

where y_{tr} is the transient response with the property that it goes to zero as τ goes to infinity, and y^* is a stable solution. As τ varies, the points (ϕ^*, y^*) moves along a trajectory. Since $\phi \in [0, 2\pi]$, it is convenient to take phase space to be the cylinder. Since the system is dissipative, there are only two

kinds of motion on the cylinder [5], as shown in Fig. 4. Fig. 4a corresponds to the rotation motion of the pendulum. The motion is the same when ϕ differs by 2π. This motion occurs when ρ exceeds a specific value, which will be studied in (2.2.4). Fig. 4b corresponds to the dissipative motion of the pendulum, it will stop at some point eventually. This point is called the "fixed point" of (2.7), which will be studied in (2.2.3).

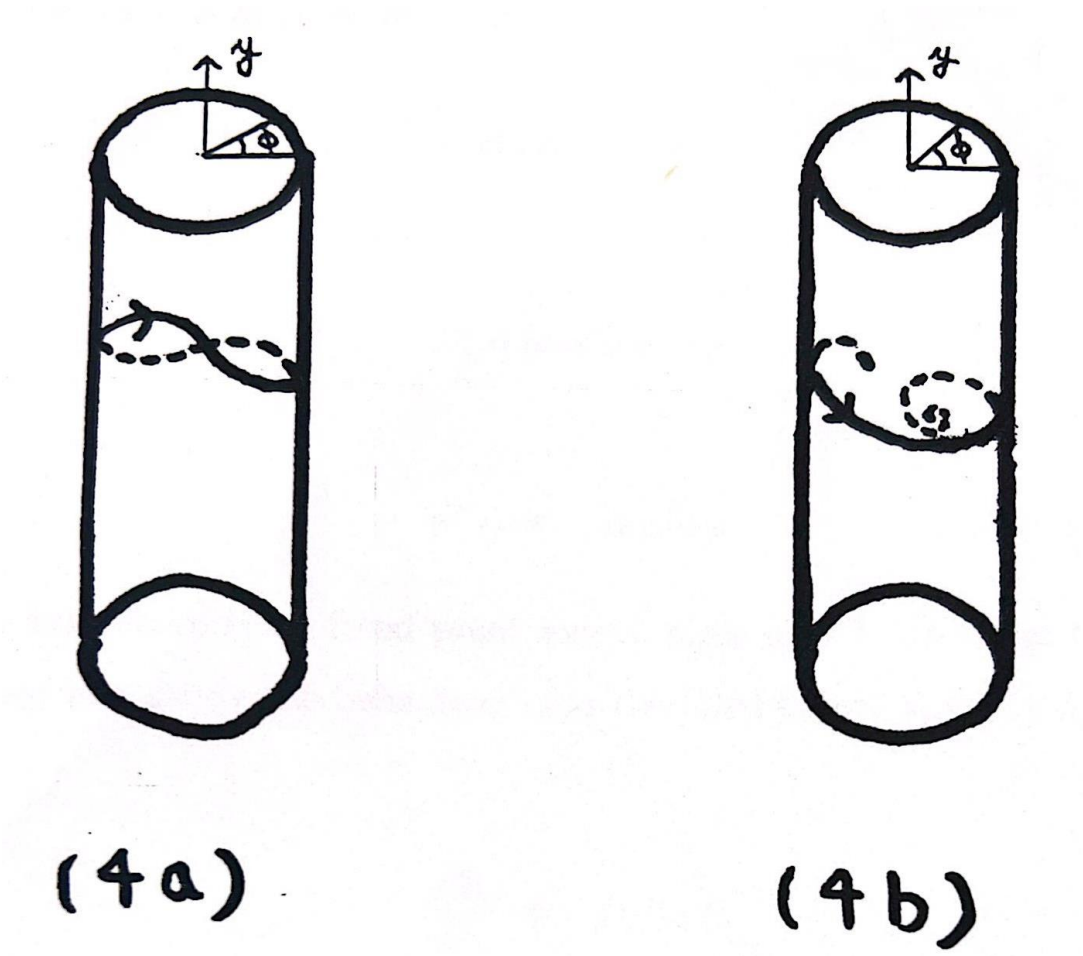

2.2.2 Symmetry

If we let

$$\phi \to -\phi,$$
$$\rho \longrightarrow -\rho.$$

(2.5) becomes

$$-\frac{d^2\phi}{d\tau^2} - \frac{1}{\sqrt{\beta}}\frac{d\phi}{d\tau} - \sin\phi = -\rho,$$

then

$$\frac{d^2\phi}{d\tau^2} + \frac{1}{\sqrt{\beta}}\frac{d\phi}{d\tau} + \sin\phi = \rho$$

It is the same as (2.5). It follows that only the range $\rho \geq 0$ needs consideration.

2.2.3 Fixed points

The fixed point of (2.5) is at $\phi^* = y^* = 0$,

such that

$$-\sin\phi^* + \rho = 0,$$

and

$$\phi^* = \sin^{-1}\rho > 0,$$

or

$$\phi^* = \pi - \sin^{-1}\rho \tag{2.8}$$

From (2.8), we find there is no fixed point exists when $\rho > 1$. In order to study the phase portrait, we must also study the behavior near the fixed point. Write (2.6) as [3], [4], [7]

$$\begin{cases} \frac{d\phi}{d\tau} = f(\phi, y), \\ \frac{dy}{d\tau} = g(\phi, y), \end{cases} \tag{2.9}$$

where

$$f(\phi, y) = y,$$

$$g(\phi, y) = \rho - \frac{y}{\sqrt{\beta}} - \sin\phi,$$

and let

$$\varepsilon_1 = \phi - \phi^*,$$

$$\varepsilon_2 = y - y^*.$$

Substituting into (2.9) and neglecting ε^2 terms, we get [7]

$$\begin{bmatrix} \frac{d\varepsilon_1}{dt} \\ \frac{d\varepsilon_2}{dt} \end{bmatrix} = \begin{bmatrix} \frac{\partial f}{\partial \phi} & \frac{\partial f}{\partial y} \\ \frac{\partial g}{\partial \phi} & \frac{\partial g}{\partial y} \end{bmatrix} \begin{bmatrix} \varepsilon_1 \\ \varepsilon_2 \end{bmatrix}, \tag{2.10}$$

where

$$\begin{bmatrix} \frac{\partial f}{\partial \phi} & \frac{\partial f}{\partial y} \\ \frac{\partial g}{\partial \phi} & \frac{\partial g}{\partial y} \end{bmatrix} = \begin{bmatrix} 0 & 1 \\ -\cos\phi^* & -\frac{1}{\sqrt{\beta}} \end{bmatrix} \tag{2.11}$$

In general, we would like to find out the trajectories of (2.10) which gives the time evolution of ε_1 and ε_2

$$\begin{bmatrix} \varepsilon_1 \\ \varepsilon_2 \end{bmatrix} = e^{\lambda\tau} \begin{bmatrix} v_1 \\ v_2 \end{bmatrix} \tag{2.12}$$

Substitute (2.12) into (2.10), the eigenvalue λ of (2.10) is

$$\lambda = \frac{-\frac{1}{\sqrt{\beta}} \pm \sqrt{\frac{1}{\beta^2} - 4\cos\phi^*}}{2} \tag{2.13}$$

The general solution of (2.10) is

$$\begin{bmatrix} \varepsilon_1 \\ \varepsilon_2 \end{bmatrix} = C_1 e^{\lambda_1\tau} \begin{bmatrix} u_1 \\ u_2 \end{bmatrix} + C_2 e^{\lambda_2\tau} \begin{bmatrix} v_1 \\ v_2 \end{bmatrix}$$

where C_1, C_2 are determined by initial conditions. Substituting (2.8) into (2.13), we have three kinds of fixed points

1. $\cos\phi^* = \cos(\sin^{-1}\rho) > 0$, and $\frac{1}{\beta^2} - 4\cos\phi^* > 0$. The eigenvalues are real and negative. The fixed point is a stable node, any trajectories near this point will tend to this node as $\tau \to \infty$.
2. $\cos\phi^* = \cos(\sin^{-1}\rho) > 0$, but $\frac{1}{\beta^2} - 4\cos\phi^* < 0$. The eigenvalues are complex conjugate. The fixed point is a stable spiral.
3. $\cos\phi^* = \cos(\sin^{-1}\rho) < 0$. The eigenvalues are real and have opposite sign. The fixed point is a saddle point.

All three kinds of fixed points are shown in Fig.5.

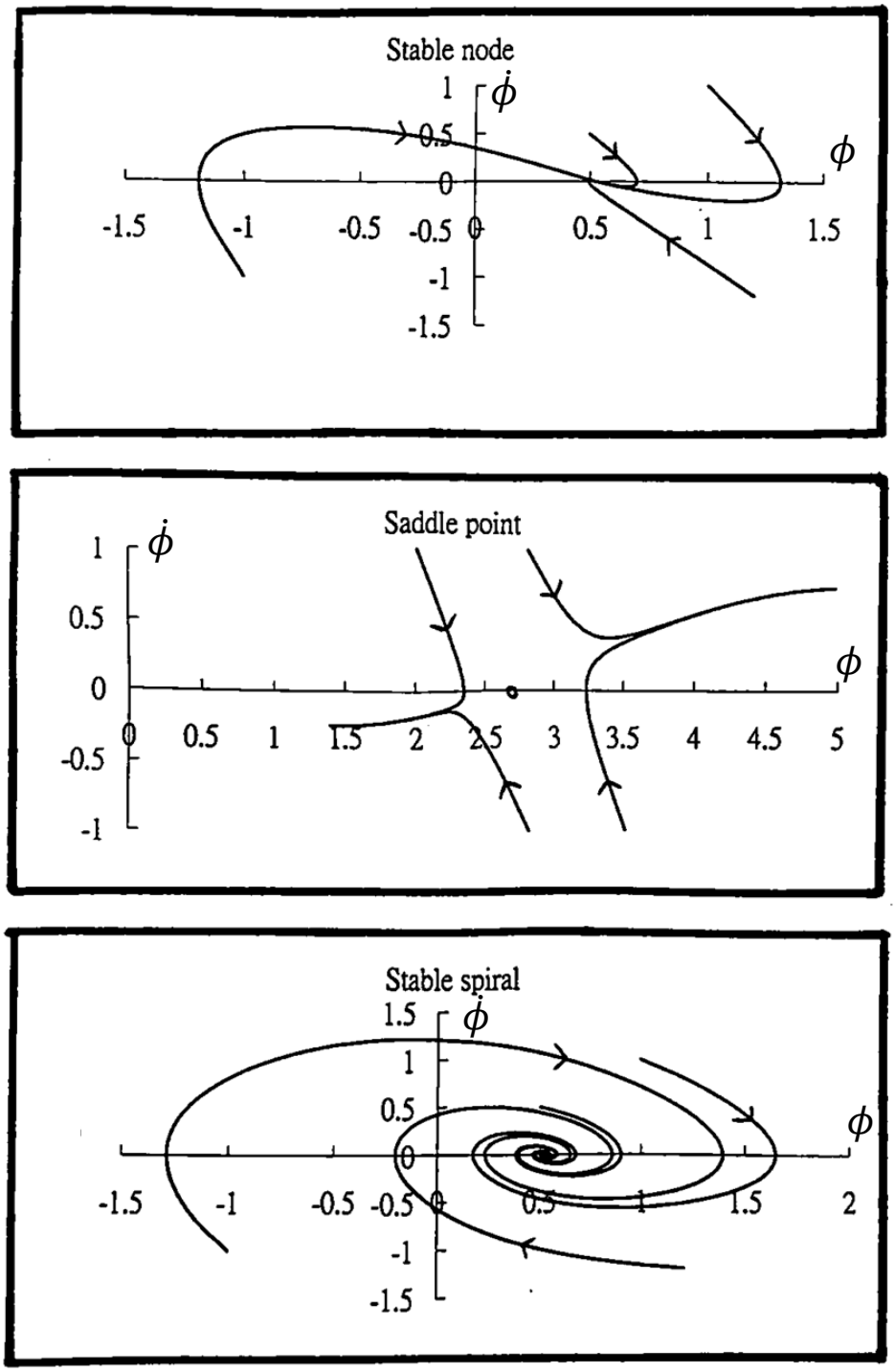
Stable node
$\dot{\phi}$
ϕ
1
0.5
0
-0.5
-1
-1.5
-1.5
-1
-0.5
0
0.5
1
1.5
Saddle point
$\dot{\phi}$
ϕ
1
0.5
0
-0.5
-1
0
0.5
1
1.5
2
2.5
3
3.5
4
4.5
5
Stable spiral
$\dot{\phi}$
ϕ
1.5
1
0.5
0
-0.5
-1
-1.5
-1.5
-1
-0.5
0
0.5
1
1.5
2

Fig.5

2.2.4 Bifurcation analysis

We now use Melnikov function [1] to calculate the bifurcation of the autonomous system

$$\begin{cases} \frac{d\phi}{d\tau} = y, \\ \frac{dy}{d\tau} = \rho - \frac{y}{\sqrt{\beta}} - \sin\phi \end{cases}$$

Let $\rho - \frac{y}{\sqrt{\beta}}$ be a perturbation,

$$\begin{cases} \frac{d\phi}{d\tau} = y, \\ \frac{dy}{d\tau} = -\sin\phi + \varepsilon\left(\rho - \frac{y}{\sqrt{\beta}}\right), \end{cases} \tag{2.14}$$

where $0 < \varepsilon \ll 1$

The unperturbed system is a Hamiltonian [4]

$$\begin{cases} \frac{d\phi}{d\tau} = y, \\ \frac{dy}{d\tau} = -\sin\phi. \end{cases} \tag{2.15}$$

From (2.15), the Hamiltonian of the system is

$$H = \frac{1}{2}\left(\frac{d\phi}{d\tau}\right)^2 + (1 - \cos\phi),$$

as shown in the following diagram

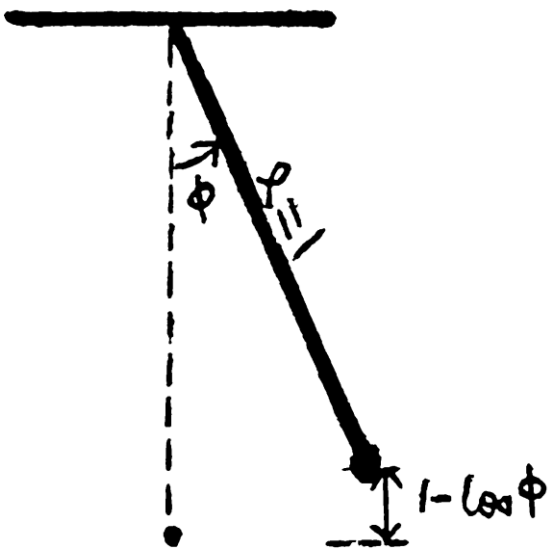

The energy of the homoclinic orbit is

$$H = \frac{1}{2}(\frac{d\phi}{d\tau})^2 + (1 - \cos\phi) = 2,$$

then

$$\frac{d\phi}{d\tau} = \pm\sqrt{2(1+\cos\phi)}$$

gives

$$\begin{cases} \phi_{\pm}^{0}(\tau) = \pm 2\tan^{-1}(\sinh\tau) \\ y_{\pm}^{0}(\tau) = \pm 2\,\mathrm{sech}(\tau) \end{cases} \tag{2.16}$$

The Melnikov function [1] is

$$M^{\pm}\left(\rho, \frac{1}{\sqrt{\beta}}\right) = \int_{-\infty}^{\infty} y_{\pm}^{0}(\tau)\left[\rho - \frac{y_{\pm}^{0}(\tau)}{\sqrt{\beta}}\right] d\tau$$

Substituting (2.16) into $M^{\pm}$, we get

$$\begin{aligned} M^{+}\left(\rho, \frac{1}{\sqrt{\beta}}\right) &= \int_{-\infty}^{\infty} 2\,\mathrm{sech}\,\tau\,(\rho - \frac{1}{\sqrt{\beta}} \cdot 2\,\mathrm{sech}\,\tau)\,d\tau \\ &= \textstyle\int_{-\infty}^{\infty} \frac{d\phi}{d\tau} d\tau\rho - \frac{1}{\sqrt{\beta}} \int_{-\infty}^{\infty} 4\,\mathrm{sech}^2\tau\,d\tau \\ &= \int_{-\pi}^{\pi} \rho d\phi - \frac{4}{\sqrt{\beta}} \int_{-\infty}^{\infty} \mathrm{sech}^2\tau\,d\tau \\ &= 2\pi\rho - \frac{8}{\sqrt{\beta}} \end{aligned}$$

$$\begin{aligned} M^{-}\left(\rho, \frac{1}{\sqrt{\beta}}\right) &= \int_{\pi}^{-\pi} \rho d\phi - \frac{4}{\sqrt{\beta}} \int_{-\infty}^{\infty} \mathrm{sech}^2\tau\,d\tau \\ &= -2\pi\rho - \frac{8}{\sqrt{\beta}} \end{aligned}$$

So M^{+} has a simple zero at

$$\rho = \rho_c = \frac{4}{\pi\sqrt{\beta}}$$

and $M^{-} < 0$ for all ρ and $\frac{1}{\sqrt{\beta}}$. We conclude that

1. There is a homoclinic bifurcation when $\rho = \rho_c = \frac{4}{\pi\sqrt{\beta}} < 1$.
2. Since $M^{-} \neq 0$ all the time, no bifurcation occurs for $\rho < 1$.

The phase portraits are shown in Fig.6.

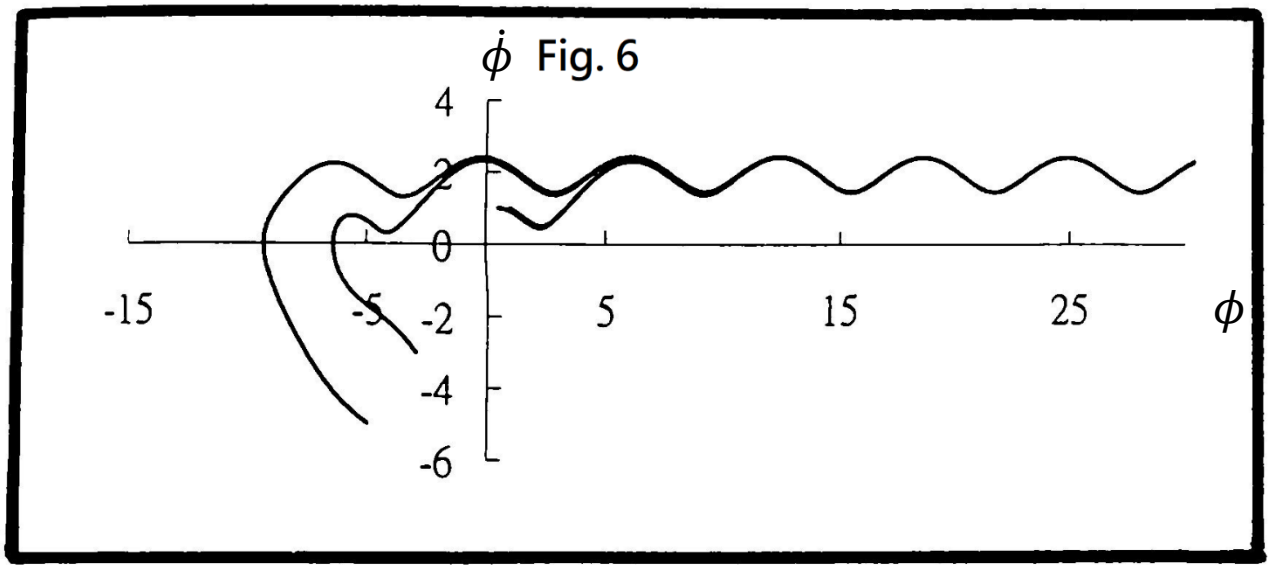

Fig. 6

We see that after bifurcation, there always exists a stable limit cycle attracts the whole phase cyclinder in the upper plane of Fig. 6. As $\rho > 1$, there is only one stable steady state solution.

However, for large $\frac{1}{\sqrt{\beta}}$, i.e., $\frac{4}{\pi\sqrt{\beta}} > 1$, we will have no homoclinic bifurcation. The fixed point attracts the whole phase cyclinder until $\rho > 1$. When $\rho = 1$ and $\rho_c < 1$, there is a saddle-node bifurcation of fixed point, and the pendulum jumps into a nonzero angular velocity state. A stable limot cycle attracts the whole phase plane as shown in Fig. 7.

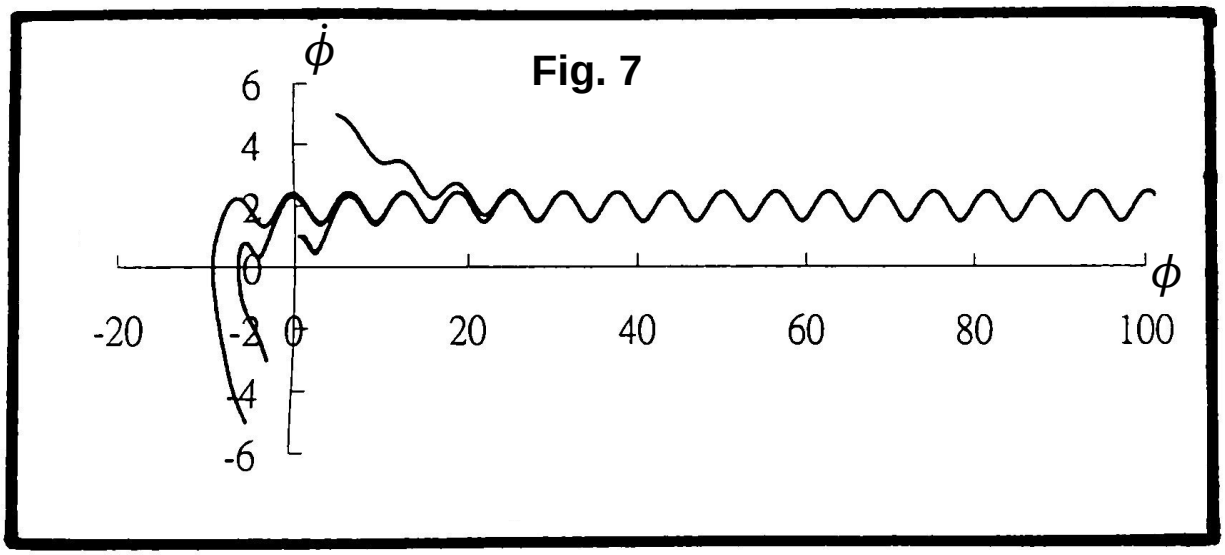

Fig. 7

2.2.5 $\rho - \dot{\phi}$ curve

The averaged angular velocity of the pendulum is determined by the following equation

$$\dot{\phi} = \omega_0 < \frac{d\phi}{d\tau} > \tag{2.17}$$

There are two critical cases:

1. When all trajectories are attracted by the fixed point. No bifurcation takes place for $\rho < 1$.

   $$< \frac{d\phi}{d\tau} > = 0$$

   This is the zero averaged angular velocity branch.

2. When $\rho \geq 1$, all trajectories will be attracted by an unique stable limit cycle. So the relation between $\dot{\phi}$ and ρ is one to one. Also, as $\rho = 1$ and $\rho_c < 1$, the pendulum will be at a saddle-node bifurcation. It will jump to an another angular velocity state discontinouosly.

However, when $\frac{1}{\sqrt{\beta}}$ is sufficient small, i.e., $\frac{4}{\pi\sqrt{\beta}} < 1$ and $\rho \in (\frac{4}{\pi\sqrt{\beta}}, 1)$, the pendulum has two stable states, the stable limit cycle or the fixed point depending on the initial conditions. The trajectories on the phase cylinder are attracted by one of two steady state conditions, From Melnikov function, we know that the homoclinic bifurcation occurs for sufficient large initial value of *y*. It leads to a running solution in the unperturbed system. This condition implies the following physics: When $\rho \in (\frac{4}{\pi\sqrt{\beta}}, 1)$ and homoclinic bifurcation of limit cycle occurs, this is the hysteresis effect of the nonlinear pendulum. But as $\rho \geq 1$, all tracjectories are attraced by an unique stable limit cycle. We next calculate the slope in the finite angular velocity branch of the $\rho - \dot{\phi}$ curve.

$$\dot{\phi} = \omega_0 < \frac{d\phi}{d\tau} >$$
$$= \omega_0 \frac{2\pi}{T}$$

then

$$\frac{d\dot{\phi}}{d\rho} = \omega_0 \cdot 2\pi(-\frac{1}{T^2})(\frac{dT}{d\rho}) \tag{2.18}$$

Since

$$\frac{dT}{d\rho} < 0$$

So

$$\frac{d\dot{\phi}}{d\rho} > 0$$

So the slope of the $\rho - \dot{\phi}$ curve is positive. But what will happen when ρ decreases, and ρ approaches $\frac{4}{\pi\sqrt{\beta}} < 1$? First we argue that when $\rho = \frac{4}{\pi\sqrt{\beta}}$, the period of the limit cycle becomes infinity. This is because of the occurrence of the homoclinic bifurcation. In fact, there are characteristic scaling laws that govern the amplitude and period of the limit cycle as the bifurcation is approached. The scaling of the period in the homoclinic bifurcation case is obtained by estimating the time required for a trajectory to pass by a saddle point.

$$\rho - \frac{4}{\pi\sqrt{\beta}} \cong Ce^{-\nu T} \tag{2.19}$$

where *T* is the period of the limt cycle. From (2.19)

$$\frac{d\rho}{dT} = -\upsilon C e^{-\nu T} \tag{2.20}$$

Substituting (2.20) into (2.18)

$$\frac{d\dot{\phi}}{d\rho} = \omega_0 \cdot 2\pi\left(-\frac{1}{T^2}\right)\left(\frac{dT}{d\rho}\right)$$

$$= \omega_0 \cdot 2\pi\left(\frac{1}{T^2}\frac{1}{\upsilon C}e^{\upsilon T}\right)$$

We get

$\frac{d\dot{\phi}}{d\rho} \to \infty$ as $T \to \infty$

which says that the finite angular velocity branch has a vertical slope at $\dot{\phi} = 0$. The $\rho - \dot{\phi}$ curve for $\frac{1}{\sqrt{\beta}} = 0.5$ and $\frac{1}{\sqrt{\beta}} = 2$ are shown in Fig. 8a and Fig.8b respectively.

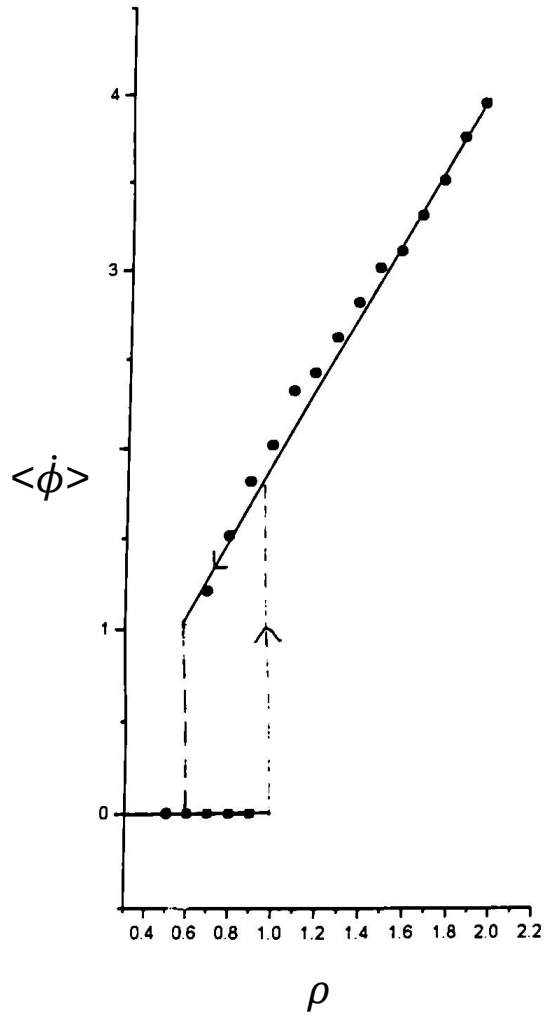

Fig. 8a

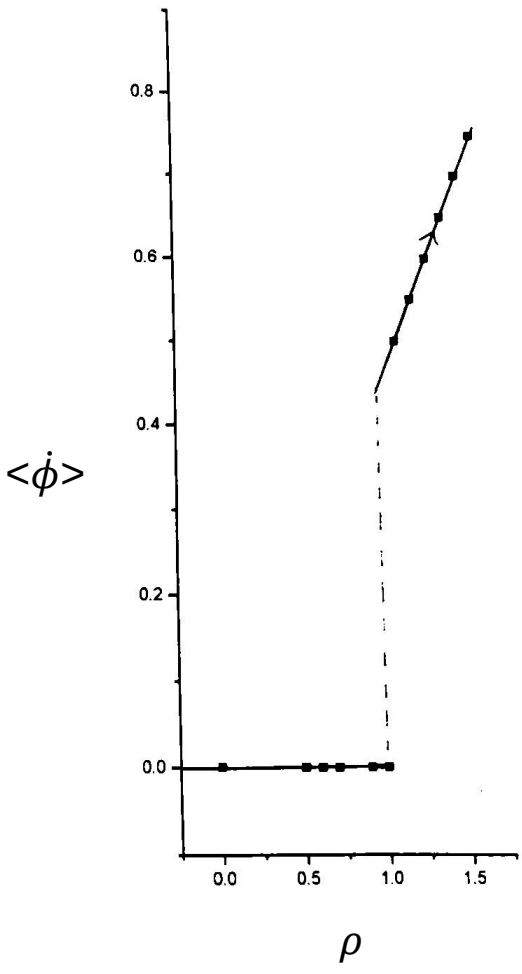

Fig. 8b

2.3 Nonautonomous case

2.3.1 Dynamical system

The equation of motion of the pendulum in the nonautonomous case is

$$\frac{d^2\phi}{d\tau^2}+\frac{1}{\sqrt{\beta}}\frac{d\phi}{d\tau}+\sin\phi=\rho+\alpha\sin\Omega\tau \tag{2.21}$$

Let

$$\frac{d\phi}{d\tau}=y$$

(2.21) becomes

$$\begin{cases}\dfrac{d\phi}{d\tau}=y,\\ \dfrac{dy}{d\tau}=\rho+\alpha\sin\theta-\dfrac{y}{\sqrt{\beta}}-\sin\phi\,,\\ \dfrac{d\theta}{d\tau}=\Omega\end{cases} \tag{2.22}$$

(2.22) describes the evolution of the dynamical system in the three dimensional space

$$I=I(\phi,y,\theta)$$

Since (2.22) is a three dimensional dynamical system, it may has chaotic behaviour. However, we only analysis non-chaotic case in this section. [5]

2.3.2 Symmetry

The system has the same symmetric behavior as in the autonomous case. So we just only need to consider the range $\rho\geq 0$.

2.3.3 Bifurcation analysis

In order to give a quantitative understand of the dynamical system, we divided the parameter space into domains. Each corresponding to a certain set of steady-state solution. Our job is to calculate the boundary of these domains by Melnikov's method and Averaging Theorem. Let $\delta=\frac{1}{\sqrt{\beta}}$, (2.21) becomes [1]

$$\begin{cases} \dfrac{d\phi}{d\tau} = y \\ \dfrac{dy}{d\tau} = -\sin\phi + \varepsilon(\rho + \alpha\sin\Omega\tau - \delta y) \end{cases} \tag{2.23}$$

Here we assume $\rho + \alpha\sin\Omega\tau - \delta y$ is a perturbation to the Hamiltonian system. The solution to the Hamiltonian system

$$\frac{d^2\phi}{d\tau^2} + \sin\phi = 0$$

Is

$$\begin{cases} \phi_{\pm}^{0}(\tau) = \pm 2\tan^{-1}(\sinh\tau) \\ y_{\pm}^{0}(\tau) = \pm 2\,\mathrm{sech}\,\tau \end{cases} \tag{2.24}$$

The corresponding Melnikov function to (2.23) is

$$M^{\pm}(\rho,\delta,\alpha) = \int_{-\infty}^{\infty} y_{\pm}^{0}(\tau)[\rho + \alpha\sin\omega(\tau+\tau_0) - \delta y_{\pm}^{0}(\tau)]d\tau \tag{2.25}$$

Substituting (2.24) into (2.25)

$$\begin{aligned} M^{\pm} &= \pm\int_{-\pi}^{\pi}\rho d\theta - 4\delta\int_{-\infty}^{\infty}\mathrm{sech}^2(\tau)d\tau \pm \alpha\int_{-\infty}^{\infty}2\,\mathrm{sech}(\tau)\sin\Omega(\tau+\tau_0)d\tau \\ &= \pm 2\pi\rho - 8\delta \pm 2\pi\alpha\sin\Omega\tau_0\,\mathrm{sech}\frac{\pi}{2}\Omega \end{aligned} \tag{2.26}$$

Where the thrid integral in $M^{\pm}$ is evaluated by the residual theorem in complex analysis. We have the bifurcation curves at

$$M = \frac{\partial M}{\partial\tau_0} = 0,$$

$$\frac{\partial^2 M}{\partial{\tau_0}^2} \neq 0.$$

So we have

$$\Omega\tau_0 = \pm\frac{\pi}{2}$$

In view of (2.26), we get if $\Omega\tau_0 = \frac{\pi}{2}$ and $\rho = \rho_c - \alpha\,\mathrm{sech}\left(\frac{\pi}{2}\Omega\right)$, then $M^+ = 0$. Since $\rho > 0$, $M^- \neq 0$. For $\Omega\tau_0 = -\frac{\pi}{2}$, $M^{\pm} = 0$ if $\rho = \pm\rho_c + \alpha\,\mathrm{sech}\left(\frac{\pi}{2}\Omega\right)$. However, we know if $\rho_c = \frac{4\delta}{\pi} \leq 1$, the maximum zero angular velocity torque is

$$\rho = 1 - \alpha\,\mathrm{sech}(\frac{\pi}{2}\Omega)$$

The bifurcation curves for the nonautonomous case is

$$\begin{cases} \rho_c^- = \rho_c - \alpha\,\mathrm{sech}\dfrac{\pi}{2}\Omega \\ \rho_c^+ = \rho_c + \alpha\,\mathrm{sech}\dfrac{\pi}{2}\Omega \\ \rho_c^0 = -\rho_c + \alpha\,\mathrm{sech}\dfrac{\pi}{2}\Omega \\ \rho^\nu = 1 - \alpha\,\mathrm{sech}\dfrac{\pi}{2}\Omega \end{cases} \tag{2.27}$$

These bifurcation curves in the parameter space for $\Omega = 1$, $\alpha = 0.5$ are shown in Fig. 9 in the $\rho, \sqrt{\beta}$ plane. Note that $\frac{1}{\sqrt{\beta}}$ is the damping term of the dynamical syatem.

Fig. 9 bifurcation curves

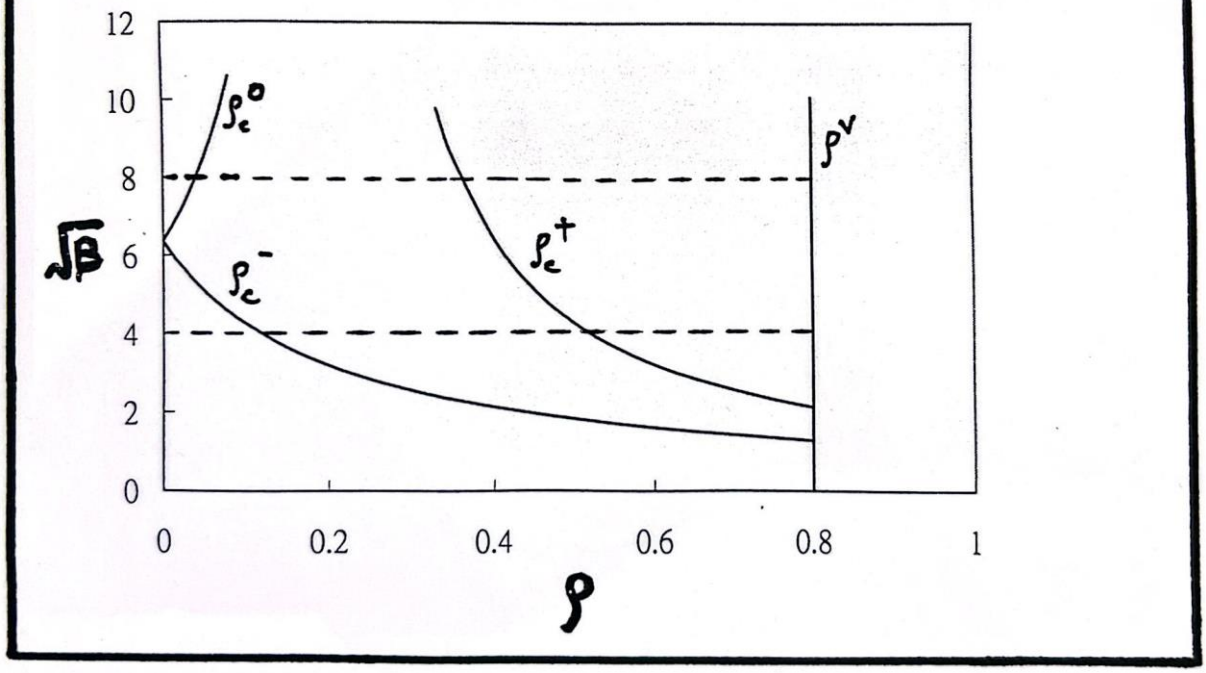

The intersection of ρ_c^- and ρ_c^0 is given by

$$\rho_c = \alpha \operatorname{sech} \frac{\pi}{2} \Omega$$

or

$$\sqrt{\beta} = \frac{4}{\pi\alpha} \cosh \frac{\pi}{2} \Omega \tag{2.28}$$

(2.28) implies that ρ_c^0 is meaningless for very damping, i.e.,

$$\sqrt{\beta} < \frac{4}{\pi\alpha} \cosh \frac{\pi}{2} \Omega$$

However, in view of Fig. 9, for $\sqrt{\beta} \ll 1$, the system can be viewed as an overdamped system. We will discuss this in the next section. For intermediate value of $\sqrt{\beta}$, the behaviour of the solution curves in the fifferent domains of the decomposition are sketched in Fig. 10.

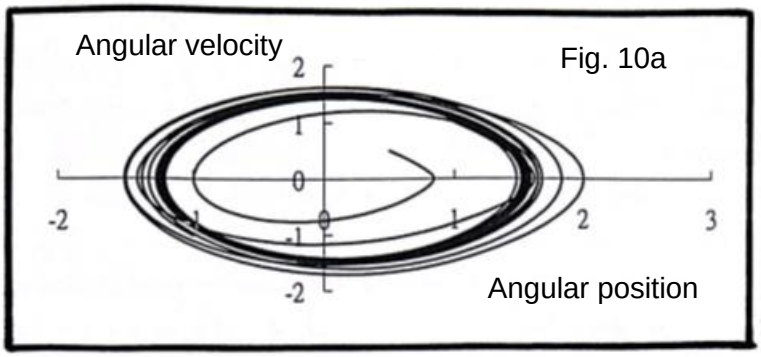

Fig. 10a

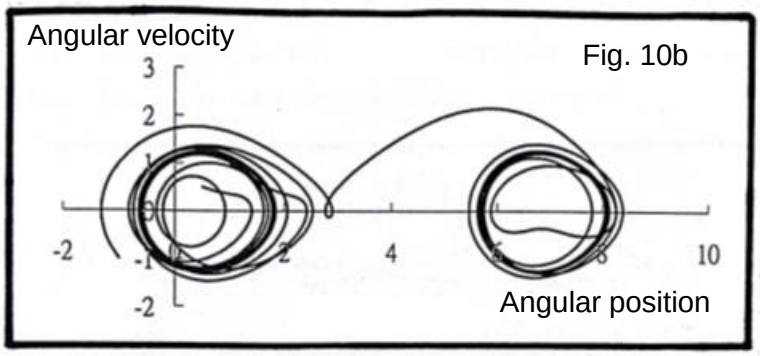

Fig. 10b

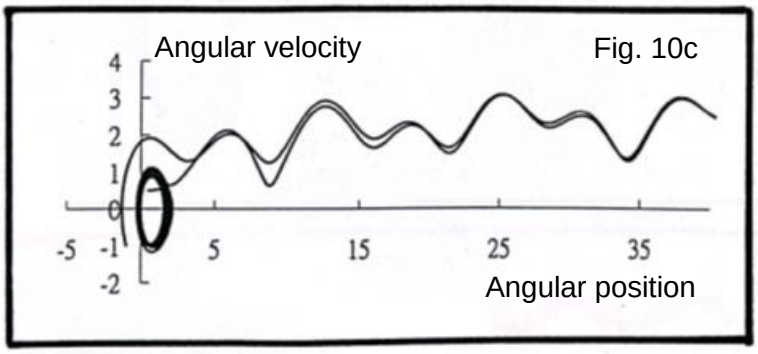

Fig. 10c

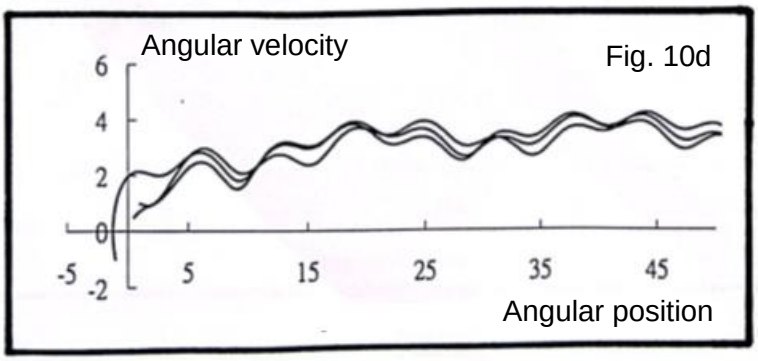

Fig. 10d

Fig. 10a implies there exists a stable limit cycle which attracts the solution curves. However, this cycle is not unique, the range of the attraction depends on the stability of each solution curve, i.e., depends on the initial conditions. When ρ increases (Fig. 10b), the attractive region becomes smaller. However, we can not find any running solution in this region for any initial conditions. As $\rho > \rho_c^+$, as in Fig. 10c, certain initial conditions lead to an unique runnimg solution, but other initial conditions are still attracted by the limit cycle, this is an oscillating solution. As $\rho > 1 - \alpha$, as in Fig. 10d, all initial conditions lead to running solutions of same point. We think such unique form comes from the uniqueness of the Melnikov's function, as in the autonomous case. This solution also produces nonzero angular velocity of the pendulum.

The pendulum behaviours for large values of $\sqrt{\beta}$ are shown in Fig. 11.

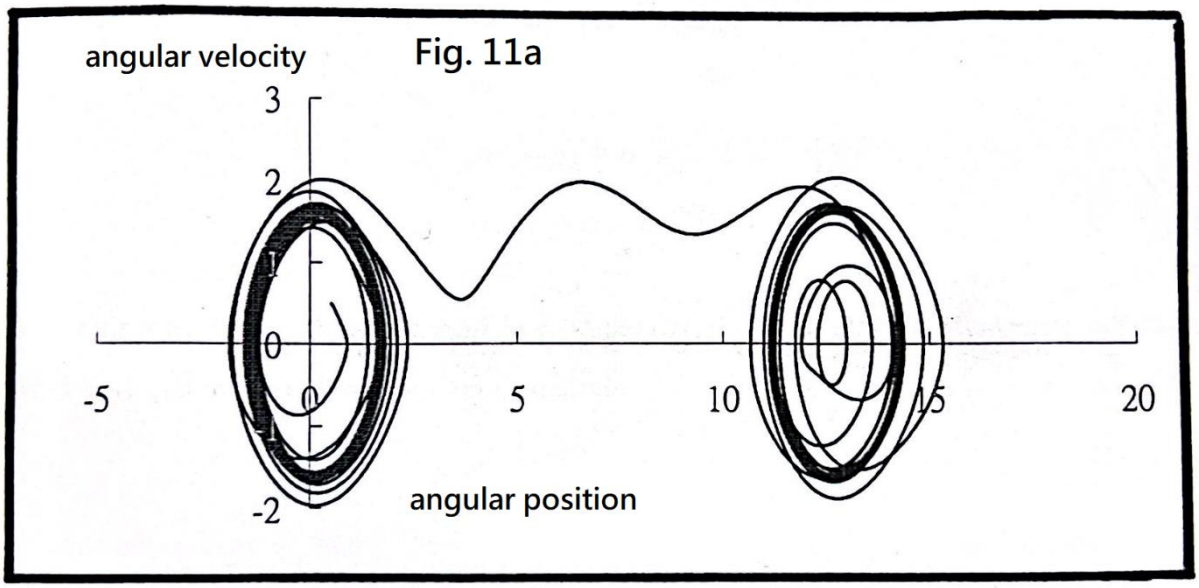

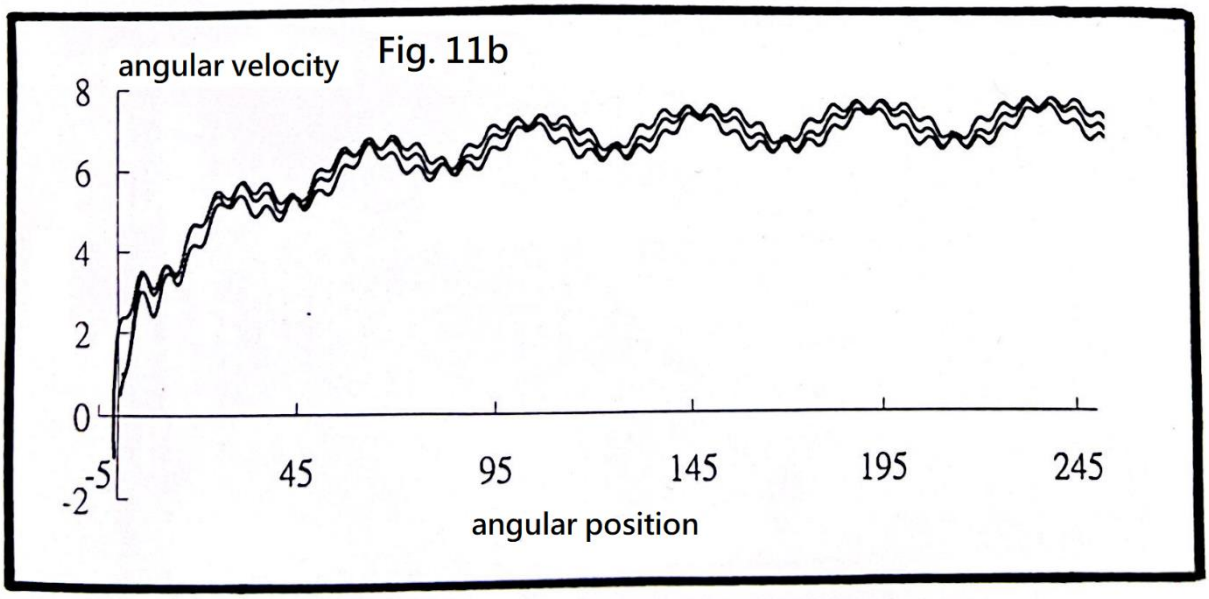

In Fig. 11a, $\rho = 0.1$. Such ρ corresponds to the case in Fig.10a, where there is a very strong attractor. But in Fig. 11a, the range of attraction becomes smaller. As $\rho > 1 - \alpha$ (Fig. 11b), all initial conditions lead to the running solution of the same point. As the same situation in Fig. 10d, this solution also produces nonzero angular velocity.

However, we also analysis the behaviour for very low and very high driving torque frequency.

a) $\Omega \to 0$.

$$\lim_{\Omega \to 0} \cosh(\frac{\pi\Omega}{2}) = 1 - o(\Omega^2)$$

(2.27) becomes

$$\begin{cases} \rho_c^- = \rho_c - \alpha - o(\Omega^2) \\ \rho_c^+ = \rho_c + \alpha + o(\Omega^2) \\ \rho_c^0 = -\rho_c + \alpha + o(\Omega^2) \\ \rho^\nu = 1 - \alpha - o(\Omega^2) \end{cases} \quad (2.29)$$

Here the maximum zero angular velocity external torque is reduced to $\rho^\nu \approx 1 - \alpha$. We illustrate the situation for $\sqrt{\beta} = 8$ and $\sqrt{\beta} = 4$ in the following diagrams.

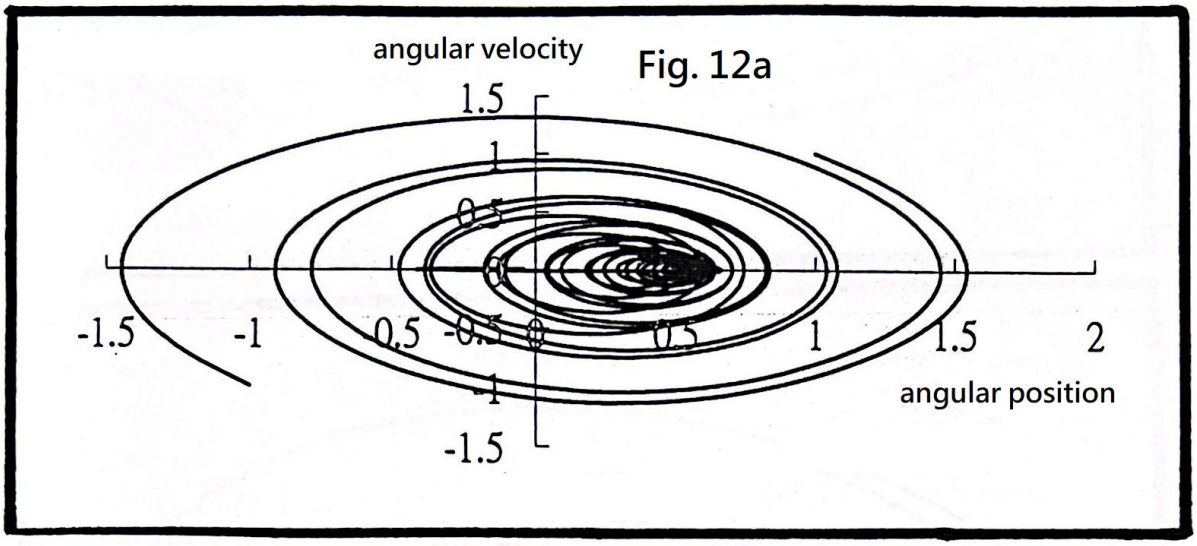

Fig. 12a

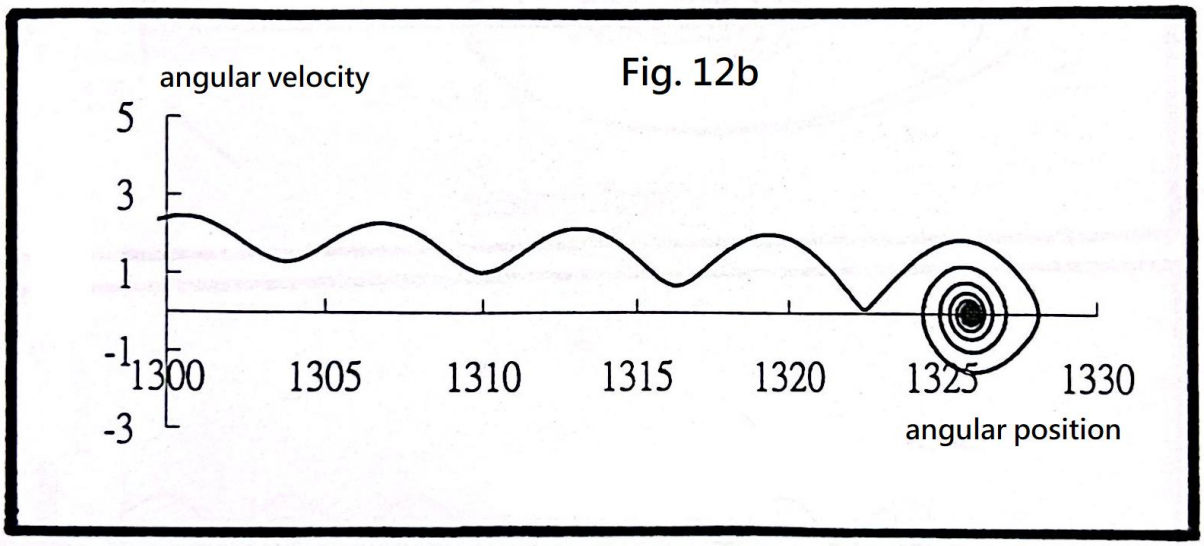

Fig. 12b

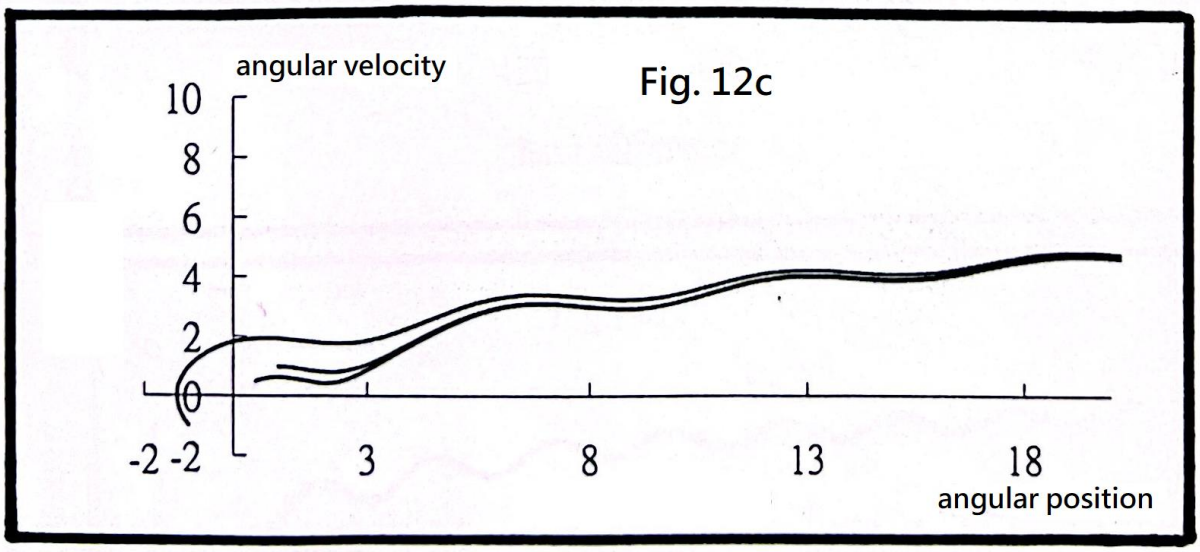

Fig. 12c

Fig. 13a

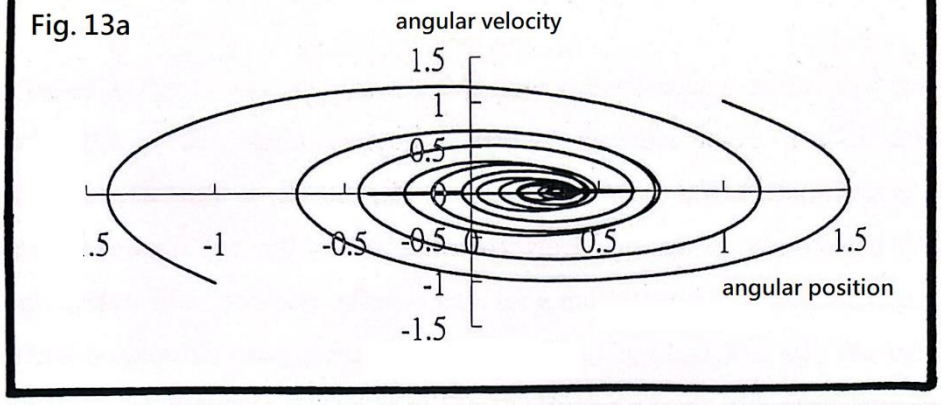

Fig. 13b

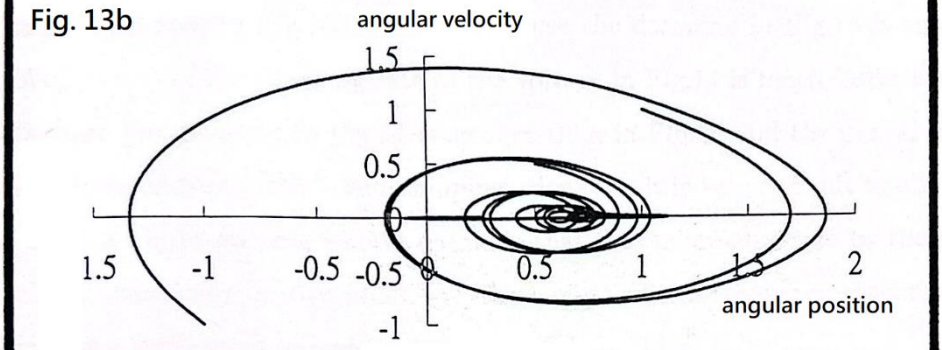

Fig. 13c

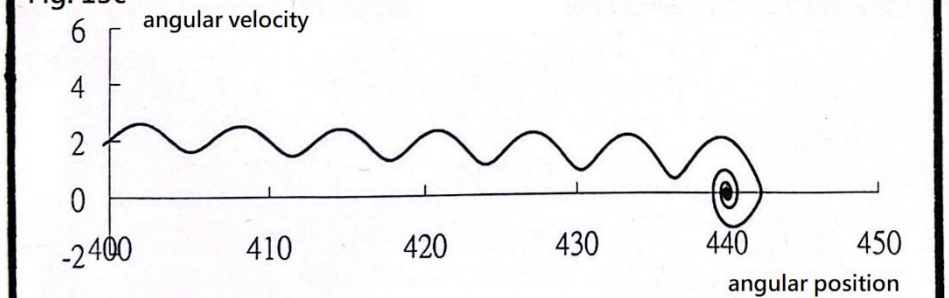

Fig. 13d

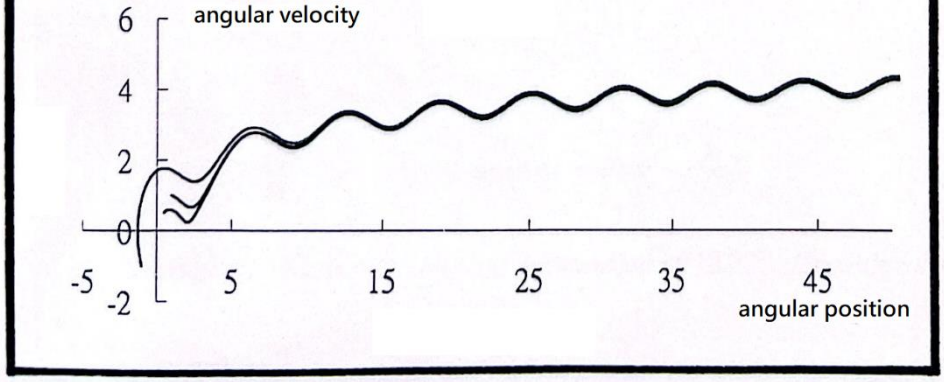

Compared to Fig. 10, the attractive stable limit cycle becomes smaller in Fig. 12 and Fig. 13, since $\operatorname{sech}\frac{\pi}{2}\Omega \cong 1$, the region between ρ_c^+ and ρ_c^- becomes larger. Fig. 13a and Fig. 13b have almost the same behavior. As $\rho > \rho_c^+$, if we keep the same initial conditions as in Fig. 10, the stronger initial conditions will lead to solutions which run longer before being attracted by the small limit cycles. The hysteresis effect occurs for a much larger initial conditions. As $\rho > 1 - \alpha$, all solutions become an unique running solution. In Fig. 12, if $\rho < \rho_c^+$, the behavior of the solution curves are almost the same as in Fig. 13. But as $\rho > \rho_c^+$, the transient effect in Fig. 12b exists longer than that in Fig. 13b. This is because the damping in Fig. 12 is small than in Fig. 13. As $\rho > 1 - \alpha$, the changing rate of the angular velocity in Fig. 12 is much faster than in Fig. 13. This is because the damping in Fig. 12 is smaller than in Fig. 13 and the period in the steady state strongly depends on both α and damping. However, it is very difficult to observe running solution both in Fig. 12 and Fig. 13. We conclude that the energy absorbed by the pendulum in very small external torque frequency is very small, i.e., there must exist a resonance region for which the pendulum absorbs the most energy from the periodic external torque.

b) For large value of Ω.

We use Average Theorem to derive the bifurcation curves. First, we change the time scale of the system.

Let

$$\tau_1 = \Omega\tau$$

and we have

$$\Omega\left(\Omega\frac{d^2\phi}{d\tau_1^2}\right) + \frac{1}{\sqrt{\beta}}\left(\Omega\frac{d\phi}{d\tau_1}\right) + \sin\phi = \rho + \alpha\sin\tau_1 \tag{2.30}$$

Then

$$\begin{cases} \dfrac{d\phi}{d\tau_1} = \dfrac{y}{\Omega} \\ \dfrac{dy}{d\tau_1} = \dfrac{1}{\Omega}\left(\rho + \alpha\sin\tau_1 - \sin\phi - \dfrac{y}{\sqrt{\beta}}\right) \end{cases} \tag{2.31}$$

Now we use Average Theorem to study the bifurcation of (2.31). We now write (2.31) as [1]

$$\begin{cases} \frac{d\phi}{d\tau_1} = \varepsilon y \\ \frac{dy}{d\tau_1} = \varepsilon(\rho + \alpha \sin\tau_1 - \sin\phi - \frac{y}{\sqrt{\beta}}) \end{cases} \tag{2.32}$$

where $\varepsilon = \frac{1}{\Omega}$. By the Average Theorem, we have

$$< \frac{dy}{d\tau_1} >= \varepsilon < \left(\rho + \alpha \sin\tau_1 - \sin\phi - \frac{y}{\sqrt{\beta}}\right) >$$

where <…> means explicit average with respect to τ_1

$$< \frac{dy}{d\tau_1} >= \varepsilon \left(\rho - \sin\phi - \frac{y}{\sqrt{\beta}}\right) \tag{2.33}$$

The average theorem tells us that the bifurcation curves of (2.32) is almost the same as (2.33). By average theorem, the bifurcation curves of (2.32) is

$$\begin{aligned} \rho_c^+ &= \rho_c + o(\Omega^{-1}) \\ \rho_c^- &= \rho_c - o(\Omega^{-1}) \\ \rho^v &= 1 - o(\Omega^{-1}) \end{aligned} \tag{2.34}$$

From (2.34), we know that the bifurcation curves are in the neighborhood of ρ_c. This means that the switch point from finite to zero angular velocity always very closes to the autonomous bifurcation curve ρ_c. The phase diagrams for $\Omega \gg 1$ are shown in Fig. 14a.

For general Ω, we know from (2.27) that if α is very large, say, larger than 1, so a small addition of ρ may result in a running solution. This will give a measurable angular velocity, as shown in Fig. 14b. If α is very small, all bifurcation curves will approach ρ_c and ρ^v will close to one.

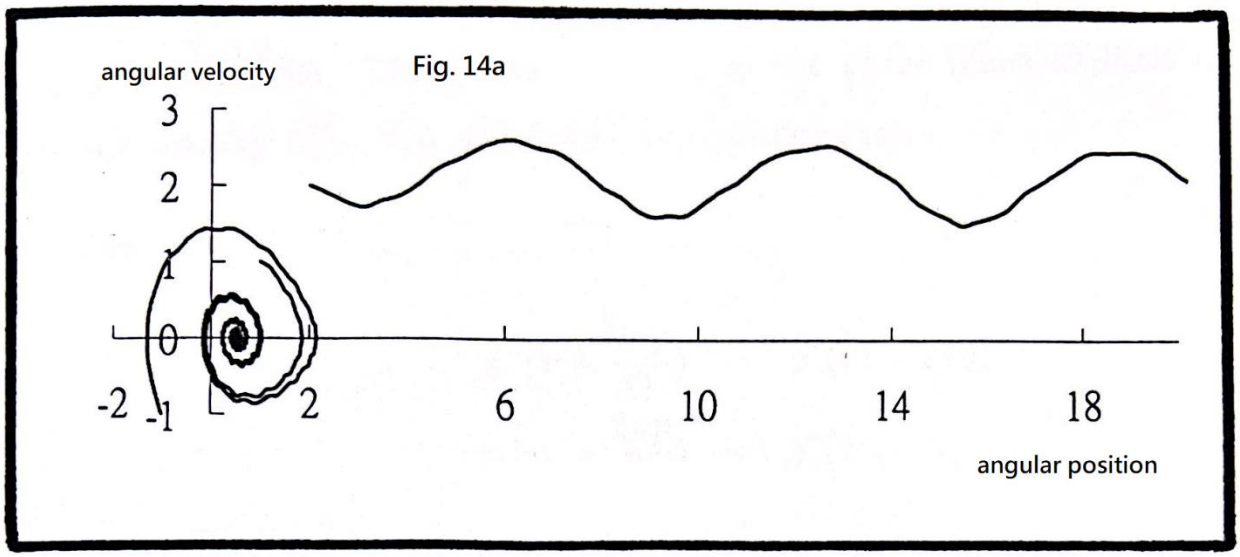

Fig. 14a

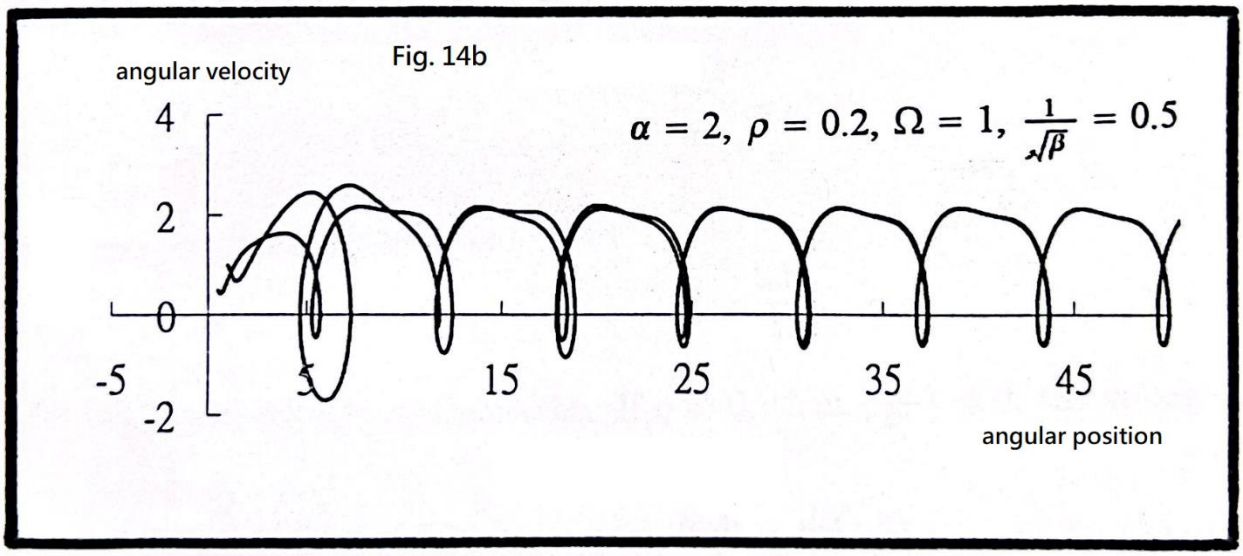

Fig. 14b

2.3.4 $\rho - \dot{\phi}$ curve

The $\rho - \dot{\phi}$ curve is determined by the steady state solution of the nonautonomous dynamical system. We have to find all equilibrium points, periodic and almost periodic solution. [3], [11]

1. Equilibrium points: These points appear in the phase plane as limit cycle, and the average velocity $< \frac{d\phi^*}{d\tau} >= 0$. It implies zero angular velocity case.
2. Periodic solution: It must satisfy the following conditions [5]:

$$\begin{aligned} \phi^*\left(\tau + \frac{2\pi p}{\Omega}\right) &= \phi^*(\tau) + 2\pi q \\ y^*\left(\tau + \frac{2\pi p}{\Omega}\right) &= y^*(\tau) \end{aligned} \tag{2.35}$$

where $(y^*(\tau), \phi^*(\tau))$ is the steady state solutions after without transient effect, and

$$\frac{d\phi^*}{d\tau} = y^*$$

The period of the solution is

$$T = \frac{2\pi p}{\Omega}$$

The average angular velocity is given by the equation

$$< \dot{\phi} >= \omega_0 < \frac{d\phi^*}{d\tau} > \tag{2.36}$$

In general

$$\begin{aligned} < \dot{\phi} > &= \omega_0 \cdot \lim_{\tau\to\infty} \frac{1}{\tau} \int_0^\tau \frac{d\phi^*}{d\tau} d\tau \\ &= \omega_0 \cdot \lim_{\tau\to\infty} \frac{\phi^*(\tau)}{\tau} \\ &= \omega r \end{aligned} \tag{2.37}$$

where

$r = \frac{q}{p}$, q and p are integers.

Thus if r is rational, the solution ϕ^* is periodic. If r is irrational, the solution ϕ^* is almost periodic and the angular velocity is given by $< \dot{\phi} > = \omega r$ for two cases.

Our next task is to calculate the whole range of the $\rho - \dot{\phi}$ curve, the dynamical system

$$\frac{d\phi^*(\tau)}{d\tau} = y^*(\tau)$$
$$\frac{dy^*(\tau)}{d\tau} = \rho + \alpha \sin \Omega\tau - \frac{y^*(\tau)}{\sqrt{\beta}} - \sin \phi^*(\tau)$$

Integrate the system from 0 to T, where T is the period of the solution or $T = \infty$ for almost periodic solution [7].

$$\int_0^T \frac{dy^*(\tau)}{\tau} d\tau = \int_0^T \left[\rho - \frac{y^*(\tau)}{\sqrt{\beta}} - \sin \phi^*(\tau)\right] d\tau - \alpha \int_0^T \sin \Omega\tau d\tau$$
$$\frac{y^*(T) - y^*(0)}{T} = \frac{1}{T}\int_0^T \left[\rho - \frac{y^*(\tau)}{\sqrt{\beta}} - \sin \phi^*(\tau)\right] d\tau - \frac{\alpha}{\Omega} \cdot \frac{1}{T}(\cos \omega T - 1) \quad (2.38)$$

So (2.37) becomes

$$0 = \rho - \frac{1}{\sqrt{\beta}} < y^*(\tau) > - < \sin \phi^*(\tau) >$$
$$\rho = \frac{< \dot{\phi} >}{\kappa} + < \sin \phi^*(\tau) >$$
$$< \dot{\phi} > = \kappa\rho - \kappa < \sin \phi^*(\tau) > \quad (2.39)$$

where $\kappa = \sqrt{\beta}\omega_0$. From (2.39), we can conclude that

1. If r is rational, $\phi^*(\tau)$ is a periodic function, $< \sin \phi^*(\tau) >$ in general does not vanish, and $< \dot{\phi} >$ may stay constant during variation of ρ.
2. If r is irrational, $\phi^*(\tau)$ is an almost periodic function, i.e., $< \sin \phi^*(\tau) > = 0$. As we shall see that the $\rho - \dot{\phi}$ curve is a straight line.
3. Since $< \sin \phi^*(\tau) > \in [-1, 1]$, the range of the $\rho - \dot{\phi}$ curve is

$$-1 + \frac{< \dot{\phi} >}{\kappa} < \rho < 1 + \frac{< \dot{\phi} >}{\kappa}$$

By (2.37), we have

$$\rho = \frac{\omega}{\omega_c} r + < \sin \phi^*(\tau) > \quad (2.40)$$

where $\omega_c = \omega_0\sqrt{\beta}$. From (2.40), for a given ρ, we can find the r- branch of the $\rho - \dot{\phi}$ curve for any fixed set of parameters $(\frac{1}{\sqrt{\beta}}, \alpha, \Omega)$. However, not all the rational r branch is stable. The stability of any specific branch under variation of ρ is determined by a variational equation.

On the basis of this discussion, the $\rho - \dot{\phi}$ curve is shown in Fig. 15 ($\frac{1}{\sqrt{\beta}} = 2$).

Angular velocity

Fig. 15

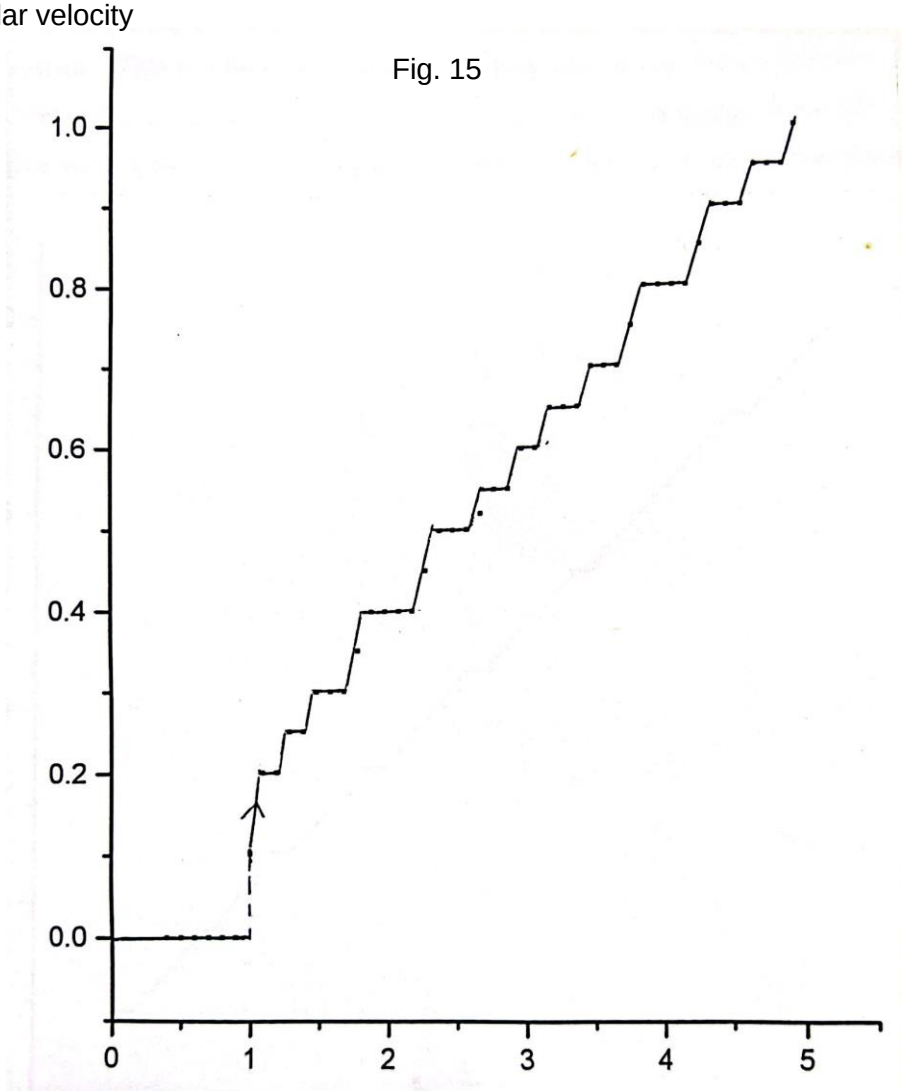

External torque

For general damping, the $\rho - \dot{\phi}$ curve is shown in Fig. 16 ($\frac{1}{\sqrt{\beta}} = 0.5$). Note that we do not neglect $\frac{d^2\phi}{d\tau^2}$. This is the inertia of the system. When ρ is reduced below 1, $\dot{\phi}$ does not drop to zero until a retrapping external torque is reached. This is a kind of bifurcation of the system, as calculated from above. However, there also exists a rotation number that characterizes the dynamical system. This *r* reflects the ratio of the frequency of the steady solution and the applied periodic torque. If *r* is rational, $< \sin\phi >\neq 0$. Furthermore, if *r* is stable, there must exist a step corresponds to this *r*. Otherwise, the behavior of the $\rho - \dot{\phi}$ curve obeys the linear relationship.

Angular velocity

Fig. 16

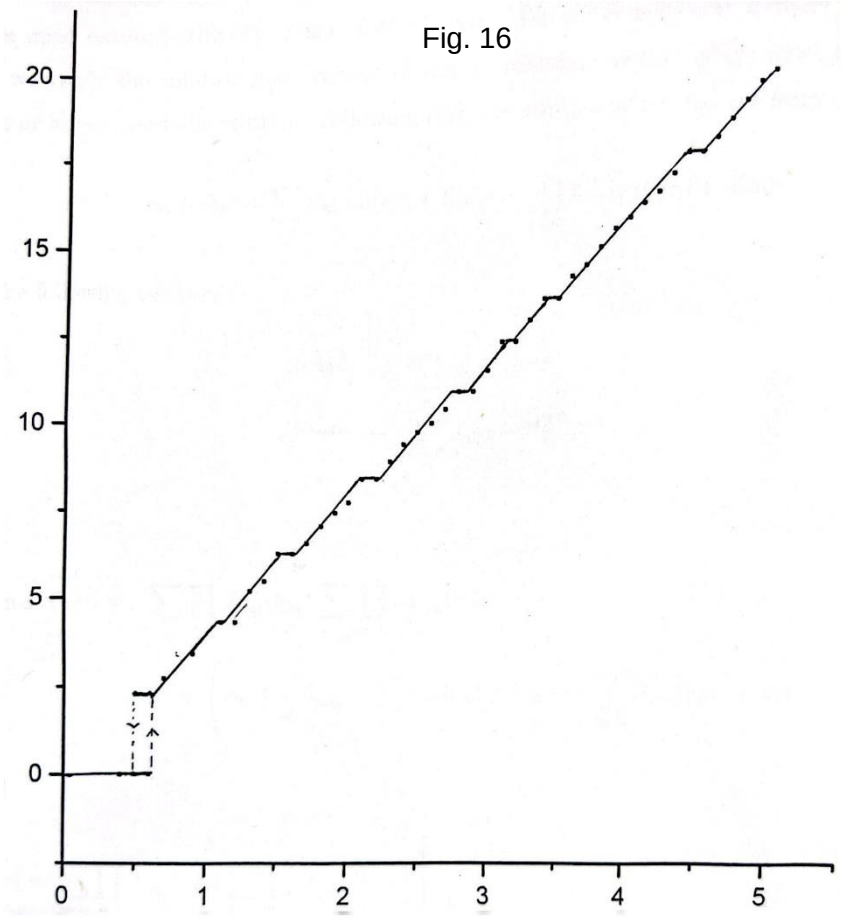

External torque

Chapter 3 Noise effect in the nonlinear pendulum system

3.1 Perturbation effect of small noise

Here we consider the system in fluctuation, we treat the fluctuation as a white noise term in the system. The equation of motion:

$$\frac{d^2\phi}{d\tau^2}+\frac{1}{\sqrt{\beta}}\frac{d\phi}{d\tau}+\sin\phi=\rho+\alpha\sin\Omega\tau+\sqrt{2D}\sigma(\tau) \tag{3.1}$$

where τ is the normalized time and $\sigma(\tau)$ is a white noise term and satisfies

$$<\sigma(\tau)>=0,$$
$$<\sigma(\tau_1)\sigma(\tau_2)>=\delta(\tau_1-\tau_2) \tag{3.2}$$

Here <…> means the ensemble average [7], [15], and *2D* is the strength of noise. We are interested in calculating the correlation function $<\phi(\tau_1)\phi(\tau_2)>$ of the system. Its Fourier transform gives the power spectrum. The perturbation effect of noise on $\phi(\tau)$ can be written as

$$\phi(\tau)=\phi_0^*(\tau)+\delta\phi_0^*(\tau) \tag{3.3}$$

where $\phi_0^*(\tau)$ is the solution to the nonlinear pendulum system in the noiseless case. Substituting (3.3) into (3.1) gives

$$\frac{d^2\delta\phi_0^*}{d\tau^2}+\frac{1}{\sqrt{\beta}}\frac{d\delta\phi_0^*}{d\tau}+(\cos\phi_0^*)\delta\phi_0^*=\sqrt{2D}\sigma(\tau) \tag{3.4}$$

From (3.4), we know that the autocorrelation function $\ll\delta\phi_0^*(\tau_1)\delta\phi_0^*(\tau_1+\tau)\gg$ can be written in the form [2], [11], [13]:

$$\ll\delta\phi_0^*(\tau_1)\delta\phi_0^*(\tau_1+\tau)\gg$$
$$=\frac{8D}{\Omega^2s^2}e^{-(\frac{k}{2})\tau}[\frac{1}{2(k^2+\Omega^2s^2)}(\Omega s\sin\left(\frac{s\Omega\tau}{2}-k\cos\frac{s\Omega\tau}{2}\right)+\frac{1}{2k}\cos\frac{s\Omega\tau}{2}] \tag{3.5}$$

where $k=\frac{1}{\sqrt{\beta}}$ and s is a constant. (3.5) implies the autocorrelation function $\ll\delta\phi_0^*(\tau_1)\delta\phi_0^*(\tau_1+\tau)\gg$ tends to zero as $\tau\to\infty$.

We assume $\phi_0^*(\tau_1)$ has the form [2]

$$\phi_0^*(\tau_1)\cong\phi_0+a_1\sin(\Omega\tau_1+\vartheta_1)+a_2\sin(\Omega_0\tau_1+\vartheta_1)+a_3\sin[(\Omega_0-\Omega)\tau_1+\vartheta_3]$$

The autocorrelation function

$$\begin{aligned} &\ll \phi_0^*(\tau_1)\phi_0^*(\tau_1+\tau) \gg \\ &= \phi_0^2 + \frac{a_1^2}{2}\cos\Omega\tau + \frac{a_2^2}{2}\cos\Omega_0\tau + \frac{a_3^2}{2}\cos(\Omega_0-\Omega)\tau \end{aligned} \tag{3.6}$$

where a_1, a_2 and a_3 are some constants.

and

$$\begin{aligned} &\ll \phi(\tau_1)\phi(\tau_2) \gg \\ &= \phi_0^2 + \frac{a_1^2}{2}\cos\Omega\tau + \frac{a_2^2}{2}\cos\Omega_0\tau + \frac{a_3^2}{2}\cos(\Omega_0-\Omega)\tau \\ &+ \frac{8D}{\Omega^2 s^2} e^{-(\frac{k}{2})\tau}\left[\frac{1}{2(k^2+\Omega^2 s^2)}\left(\Omega s \sin\left(\frac{s\Omega\tau}{2} - k\cos\frac{s\Omega\tau}{2}\right) + \frac{1}{2k}\cos\frac{s\Omega\tau}{2}\right]\right. \end{aligned} \tag{3.7}$$

We stimulate $< \phi(\tau_1)\phi(\tau_2) >$ and is shown in Fig. 17. Fig. 17a is the noiseless case. Fig. 17b is the very small noise case. Their power spectrum are shown in Fig. 18a and Fig. 18b respectively. The stimulated angular velocity correlation function and its power spectrum are shown in Fig. 19 and Fig. 20 respectively.

Angular position correlation function

Fig. 17a

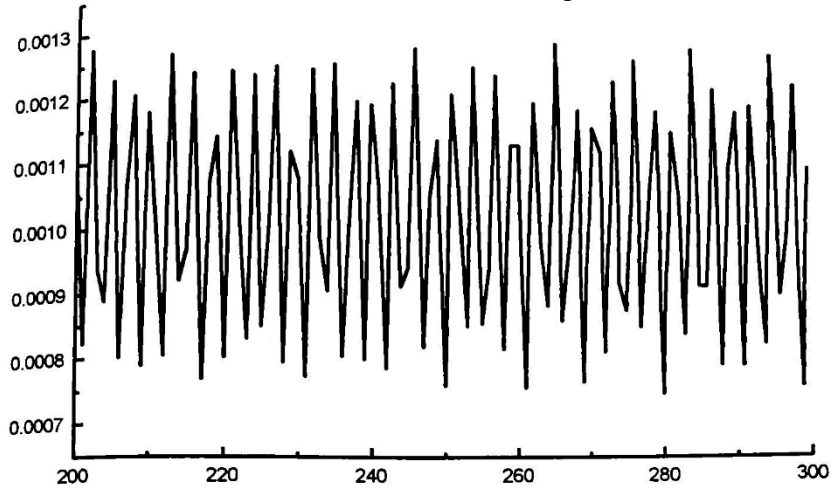

$\rho = 0.1, \alpha = 0.3, \frac{1}{\sqrt{\beta}} = 0.0004, \Omega = 2.3,$ and $D = 0$

Angular position correlation function

Fig. 17b

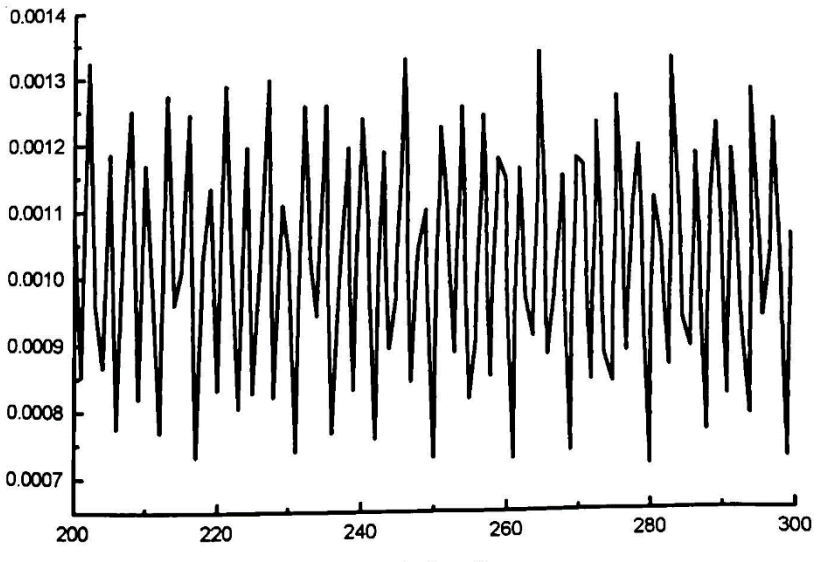

$\rho = 0.1, \alpha = 0.3, \frac{1}{\sqrt{\beta}} = 0.0004, \Omega = 2.3,$ and $D = 0.0002$

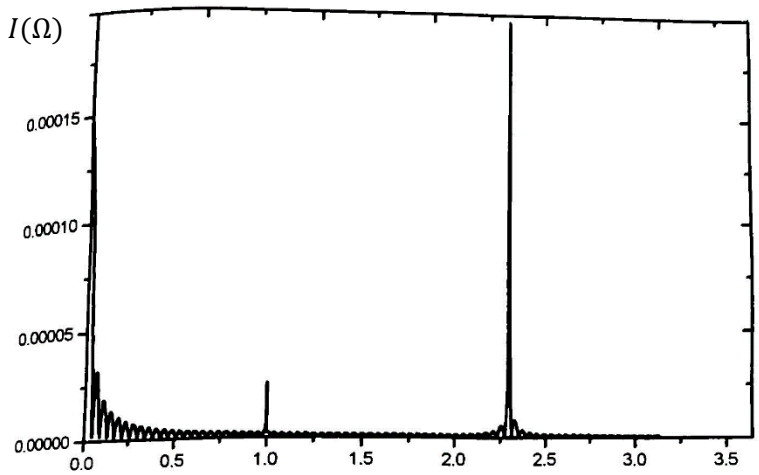

Fig. 18a

$\rho = 0.1$, $\alpha = 0.3$, $\frac{1}{\sqrt{\beta}} = 0.0004$, $\Omega = 2.3$, and $D = 0$

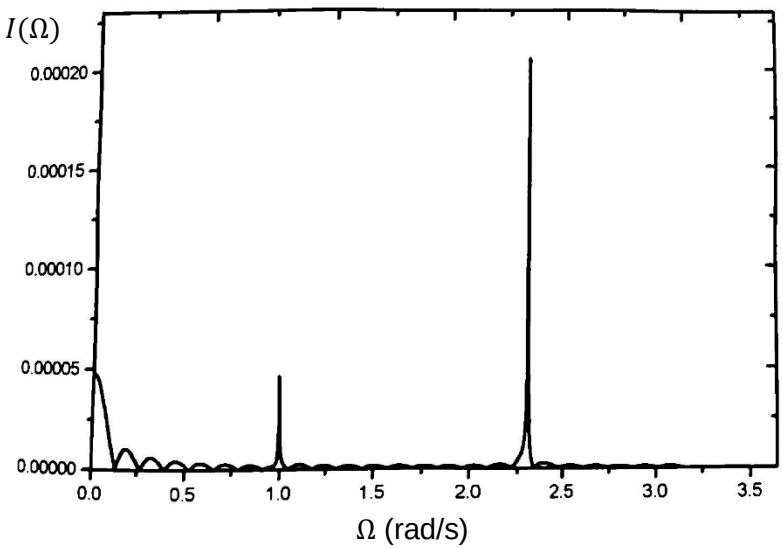

Fig. 18b

$\rho = 0.1$, $\alpha = 0.3$, $\frac{1}{\sqrt{\beta}} = 0.0004$, $\Omega = 2.3$, and $D = 0.0002$

angular velocity correlation function

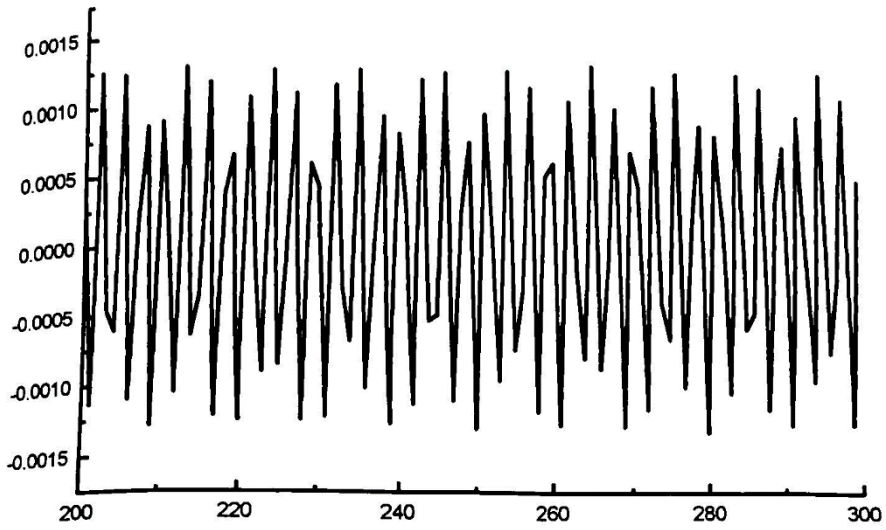

correlation time

Fig. 19a

$\rho = 0.1, \alpha = 0.3, \frac{1}{\sqrt{\beta}} = 0.0004, \Omega = 2.3,$ and $D = 0$

angular velocity correlation function

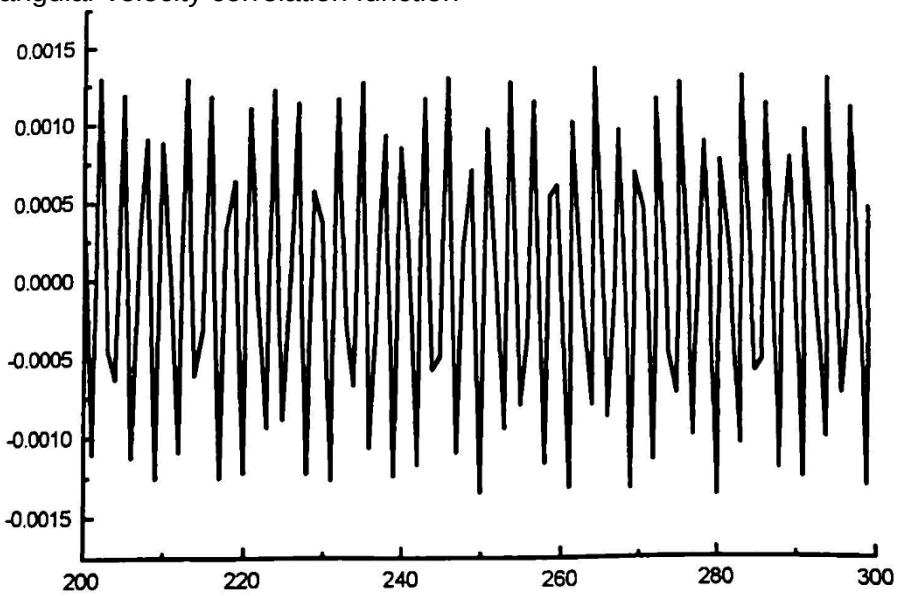

correlation time

Fig. 19b

$\rho = 0.1, \alpha = 0.3, \frac{1}{\sqrt{\beta}} = 0.0004, \Omega = 2.3,$ and $D = 0.0002$

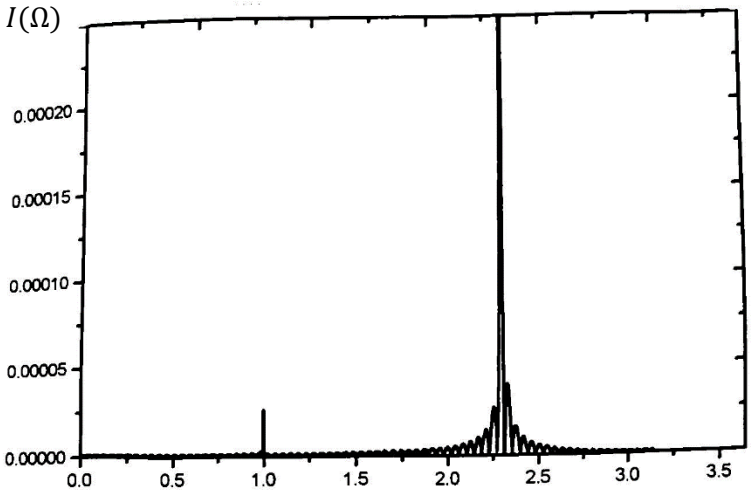

Fig. 20a

$\rho = 0.1$, $\alpha = 0.3$, $\frac{1}{\sqrt{\beta}} = 0.0004$, $\Omega = 2.3$, and $D = 0$

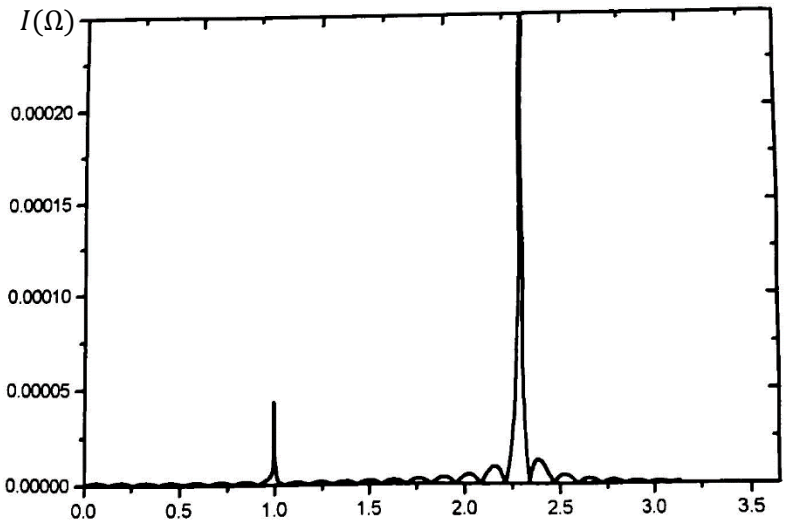

Fig. 20b

$\rho = 0.1$, $\alpha = 0.3$, $\frac{1}{\sqrt{\beta}} = 0.0004$, $\Omega = 2.3$, and $D = 0.0002$

From the above diagram, we conclude the followings:

1. There are a low frequency peak in the power spectrum of the angular position. It happens because of the nonlinear behavior of the system. Such peak is not the subharmonic oscillations of the principle frequency. It is because the nonlinear term $\sin\phi$ will give Ω any ratio of the periodic torque frequency, either almost periodic or periodic oscillations.

2. Apparently, a low peak which is stronger than the noiseless case locates in the power spectrum. This is because more energy is absorbed during the noise case.
3. However, the strength of the low frequency peaks become weaker in the angular velocity power spectrum. We explain this as follows: Consider the autocorrelation function of the Fourier transform of the angular position [7], [11], 13].

$$< \phi(\Omega_1)\phi(\Omega_2) > = \frac{1}{(2\pi)^2} < \int_{-\infty}^{\infty} e^{-i\Omega_1\tau_1}\phi(\tau_1)d\tau_1 \int_{-\infty}^{\infty} e^{-i\Omega_2\tau_2}\phi(\tau_2)d\tau_2 > \tag{3.8}$$

Let $\tau_1 - \tau_2 = \tau$ and $\frac{\tau_1+\tau_2}{2} = \tau'$. After averaging over τ_1, (3.8) becomes

$$\ll \phi(\Omega_1)\phi(\Omega_2) \gg = I(\Omega_1)\delta(\Omega_1 + \Omega_2) \tag{3.9}$$

where $I(\Omega_1)$ is the power spectrum density of the phase difference autocorrelation function. We now calculate the angular velocity power spectrum density. Its autocorrelation function is

$$< \frac{d}{d\tau_1}\phi(\tau_1)\frac{d}{d\tau_2}\phi(\tau_2) > = < \frac{d}{d\tau_1}\int_{-\infty}^{\infty} e^{-i\Omega_1\tau_1}\phi(\Omega_1)d\Omega_1 \frac{d}{d\tau_2}\int_{-\infty}^{\infty} e^{-i\Omega_2\tau_2}\phi(\Omega_2)d\Omega_2 >$$

Substituting (3.9) into above, we get

$$\begin{aligned} &< \frac{d}{d\tau_1}\phi(\tau_1)\frac{d}{d\tau_2}\phi(\tau_2) > \\ &= -\int_{-\infty}^{\infty} \Omega_1 e^{-i\Omega_1\tau_1}d\Omega_1 \int_{-\infty}^{\infty} \Omega_2 e^{-i\Omega_2\tau_2}d\Omega_2\, I(\Omega_1)\delta(\Omega_1 + \Omega_2) \\ &= \int_{-\infty}^{\infty} e^{-i\Omega_1\tau_1}\Omega_1^2 I(\Omega_1)d\Omega_1 \end{aligned} \tag{3.10}$$

So from (3.10), the power spectrum density at Ω_1 is $\Omega_1^2 I(\Omega_1)$, where $I(\Omega_1)$ is the power spectrum density of the angular position autocorrelation function. We can see that the low frequency peak becomes weaker in the angular velocity correlation function must be very small, i.e., it is very common to observe regular oscillation in angular velocity correlation function.

3.2 Stochastic Resonance

Here we study the case that the nonlinear pendulum is in an very noisy environment. There is a phenomena for which the noise will cooperate with the periodic external torque. This is called Stochastic Resonance. This effect only occurs in nonlinear dynamical systems. It will allow us to observe an usually undetectable signal. The periodic torque may be interpreted as a periodic rocking of the potential [12], [13], [14] as shown in Fig. 21.

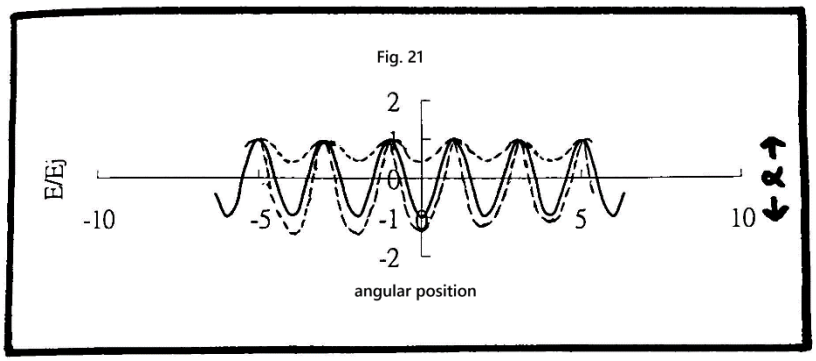

The particle is jiggled randomly by the noise. Consider the nonlinear pendulum oscillated with noise.

$$\frac{d^2\phi}{d\tau^2} + \frac{1}{\sqrt{\beta}}\frac{d\phi}{d\tau} + \sin\phi = \alpha \sin \Omega\tau + \sqrt{2D}\sigma(\tau) \tag{3.11}$$

Here we keep the damping and α very low, so the noise is not just a perturbation. There is a series of random variables $\sigma(\tau)$ having τ as a parameter. Such a time series of random variables is generally called a stochastic process. We will solve this problem by numerical method. Here we drop the constant torque term, since our main task is to investigate the periodic external torque.

3.2.1 Angular position power spectrum analysis

Here we assume the external periodic torque is too weak to cause the system to scale the potential barrier in the absence of noise. An approximate choice of the noise strength will enlarge the effect of periodic torque. It is this cooperation effect which produces escape events. Since the nonlinear pendulum system can be viewed as a multiwall system, the variation of angular position can be approximately divided into two parts. The first part characterizes the jump frequency between the wells, i.e., the escape events. The second part is the intra-well motion. The motion of the first part requires a much longer time to complete than the second part. We will study this effect in the power spectrum of

the angular position autocorrelation function. The phase diagram for the escape motion is shown in Fig. 22.

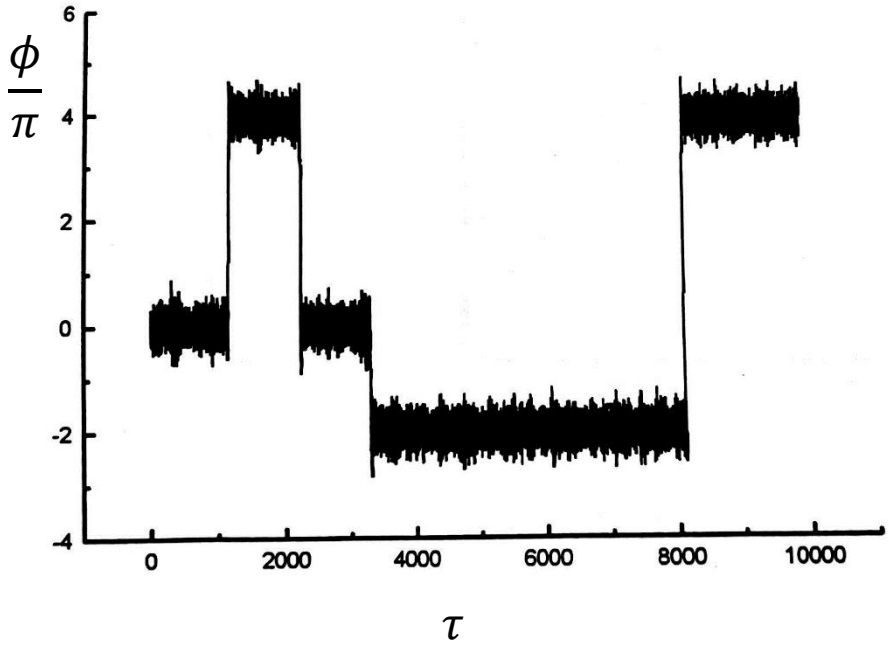

Fig . 22

$\alpha = 0.3, \Omega = 1.1, \frac{1}{\sqrt{\beta}} = 0.04, D = 1.2$

The behavior of the angular position in Fig. 22 is very different from the double well system. Once the resonance occurs, the particle will jump to a well far away. The intra-well motion is a combination effect of the periodic torque and noise. Its frequency is not simply Ω. The coherence is conveniently quantified by the power spectrum of angular position, as shown in Fig. 23a, Fig. 23b and Fig. 24, where Fig. 23a is the intra-well motion with noise and Fig. 24 is the escape motion respectively.

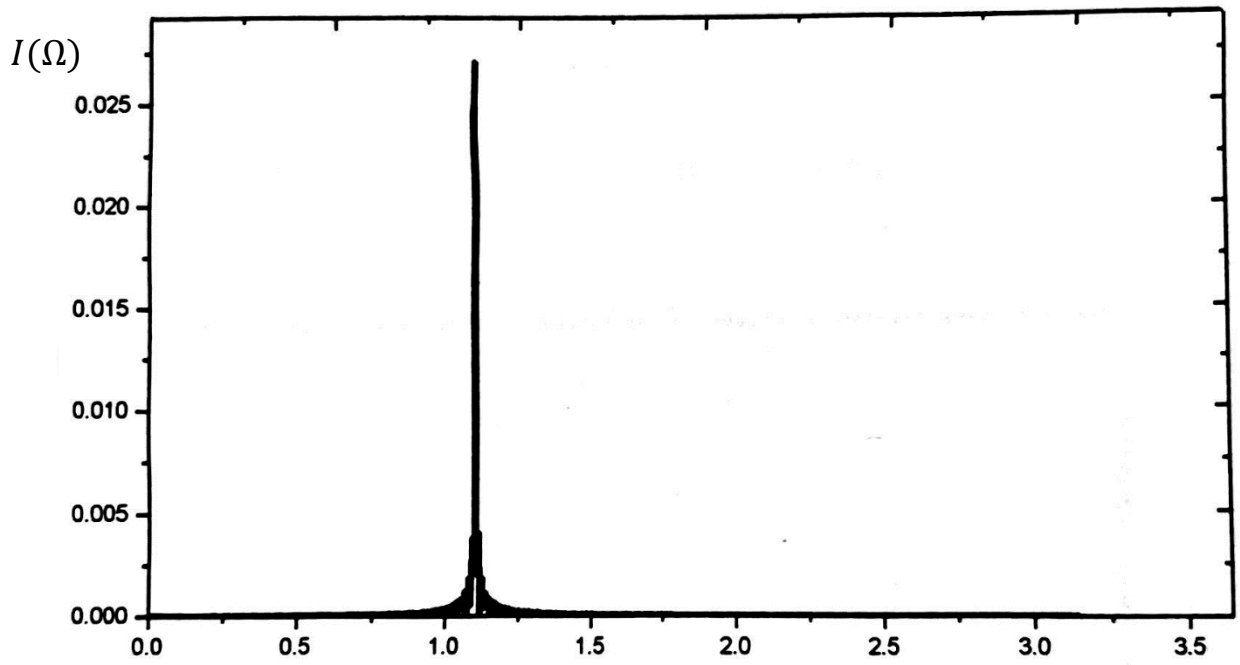

Fig. 23a

$$\alpha = 0.3, \Omega = 1.1, \frac{1}{\sqrt{\beta}} = 0.04, D = 0$$

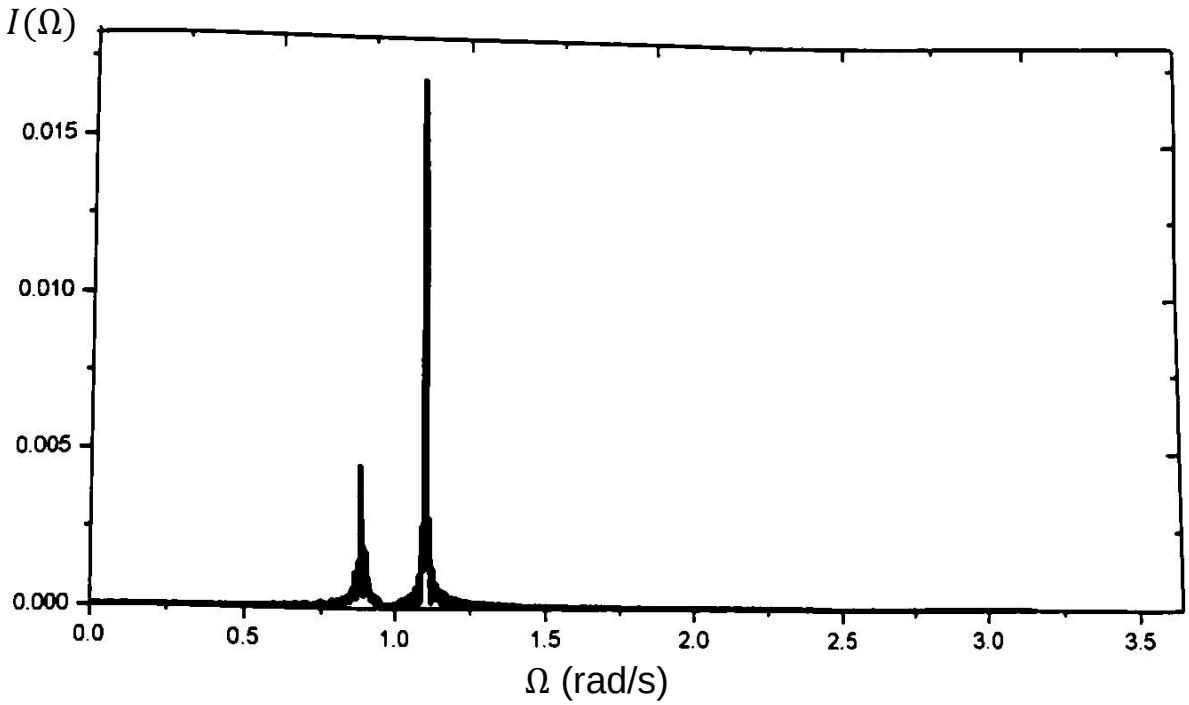

Fig. 23b

$$\alpha = 0.3, \Omega = 1.1, \frac{1}{\sqrt{\beta}} = 0.04, D = 0.75$$

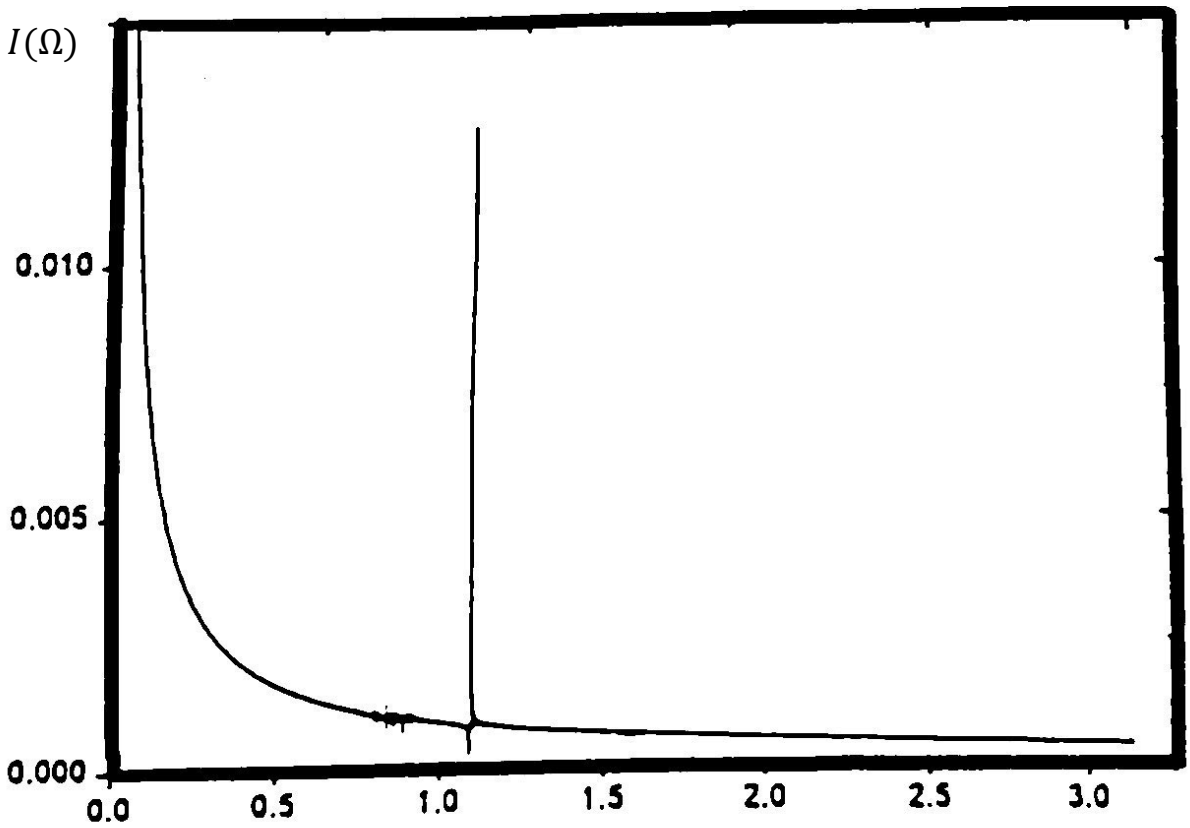

Fig. 24

$$\alpha = 0.3,\ \Omega = 1.1,\ \frac{1}{\sqrt{\beta}} = 0.04,\ D = 1.2.$$

We can draw the following conclusions from Fig. 23 and Fig.24.

1. There is a strong peak with the frequency of periodic torque in Fig. 23a.
2. There is another peak near the periodic torque frequency in Fig. 23b. This is the other harmonics which arises because of the noise and the nonlinear oscillations of the system. The strength of this peak depends on the system parameters and the initial conditions. However, when escape events occur, this peak disappears.
3. Besides the peak of the periodic torque frequency, there always exists low frequency peak in the spectrum of Fig. 24. It is because of the very small damping term. The particle may thus have many jumps before it settles down in a well. It will be a long time before the particle can make another jump. Due to the large jump, the period of the $< \phi(\tau_1)\phi(\tau_2) >$ will become very large. So there will be some very low frequency peaks appear in the power spectrum.
4. The power spectrum of Fig. 24 has a Lorentzian-like shape. The autocorrelation has the form $< \phi(\tau)\phi(0) > \cong < \phi^2 >_{st} e^{-\lambda_{min}\tau}$, where $< \phi^2 >_{st}$ is the stationary

expected value of ϕ^2 and λ_{min} is a constant value as stated in the reference [11], [15].

So

$$I(\Omega) = \frac{1}{2\pi}\int_{-\infty}^{\infty} < \phi^2 >_{st} e^{-\lambda_{min}\tau} e^{-i\Omega\tau} d\tau \qquad (3.12)$$
$$= \frac{1}{2\pi} \cdot \frac{\lambda_{min} < \phi^2 >_{st}}{\lambda_{min}^2 + \Omega^2}$$

(3.12) implies that the noise power spectrum has a Lorentzian-like distribution.

5. When the noise is too large, the cooperation disappears and the system becomes noise dominated. All escape events in this time are produced by the noise. The power spectrum of this condition is shown in Fig. 25.

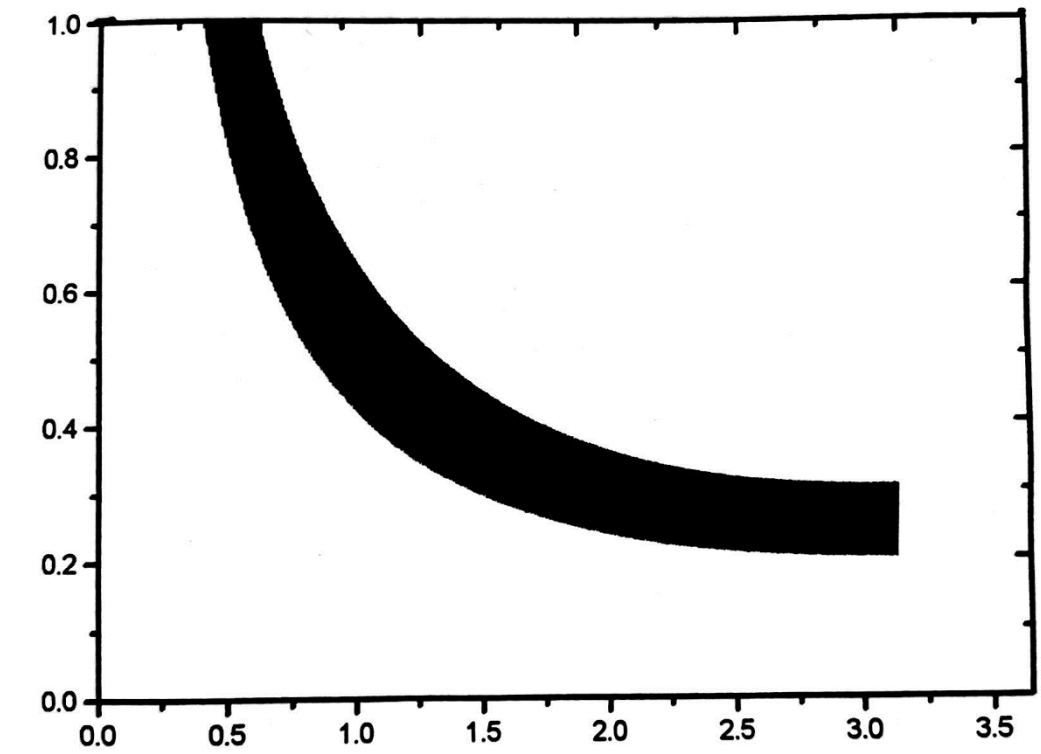

Fig. 25

$\alpha = 0.3, \Omega = 0.2, \frac{1}{\sqrt{\beta}} = 0.04, D = 2$

3.2.2 Angular velocity power spectrum analysis

The angular velocity correlation function and its power spectrum for the intra-well motion are shown in Fig. 26 and Fig. 27, where Fig. 26a and Fig. 27a are the noiseless case, Fig. 26b and Fig. 27b are the intra-well motion with noise, and for the escape motion are shown in Fig. 28 and Fig. 29. The parameters are shown in the diagrams.

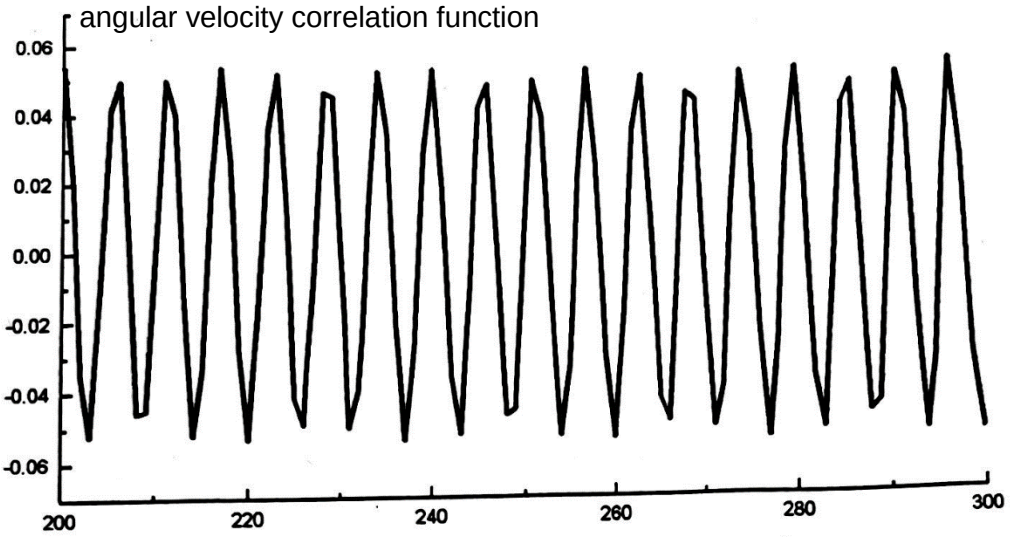

Fig. 26a

$$\alpha = 0.3, \Omega = 1.1, \frac{1}{\sqrt{\beta}} = 0.04, D = 0$$

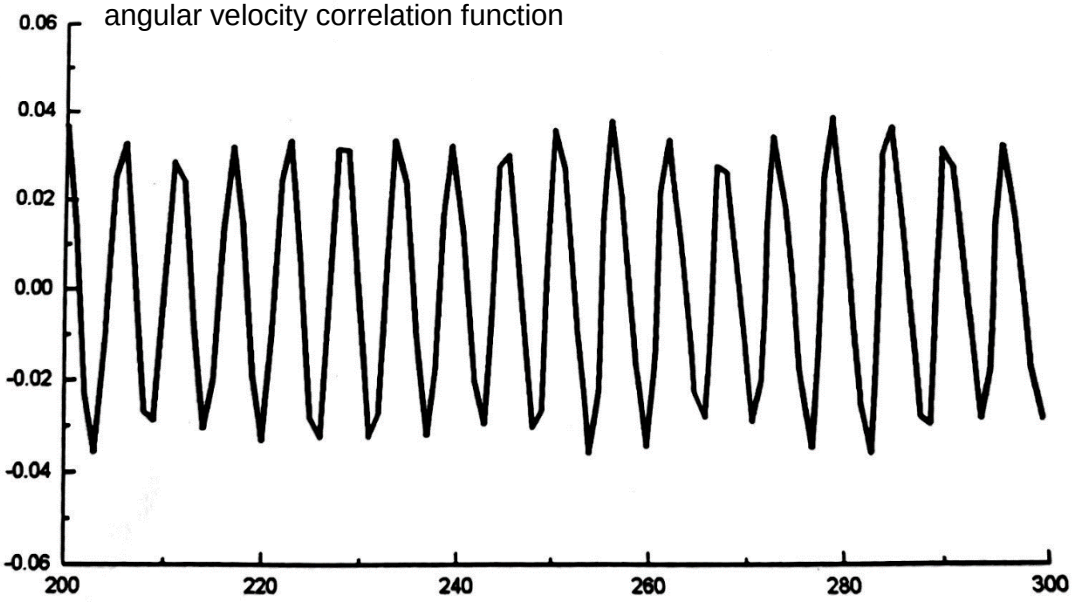

Fig. 26b

$$\alpha = 0.3, \Omega = 1.1, \frac{1}{\sqrt{\beta}} = 0.04, D = 0.75$$

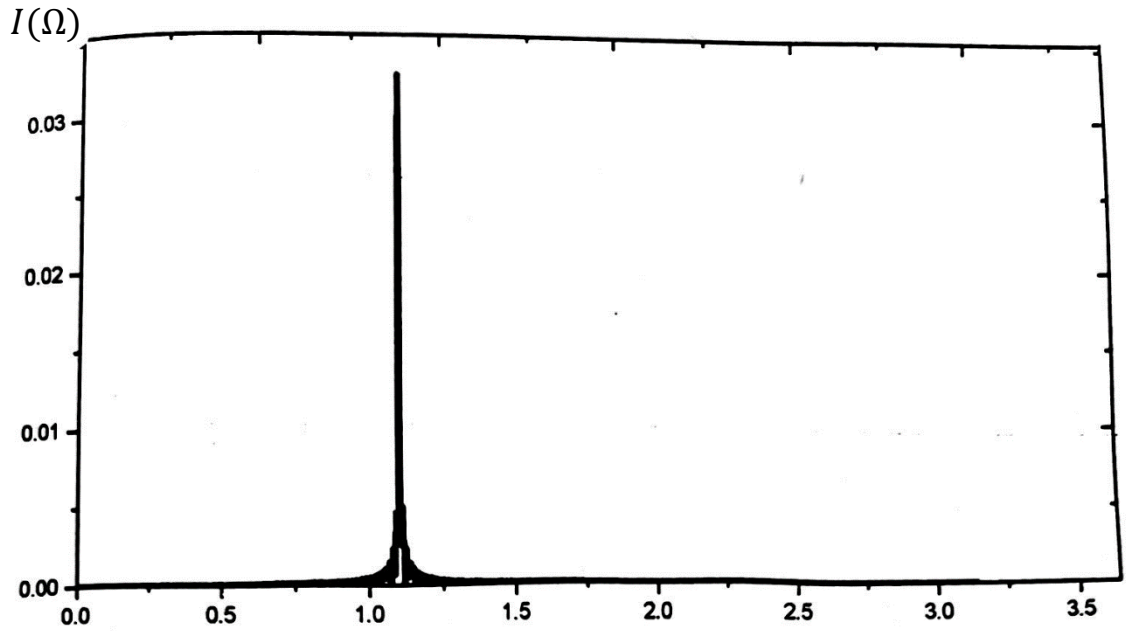

Fig. 27a

$\alpha = 0.3, \Omega = 1.1, \frac{1}{\sqrt{\beta}} = 0.04, D = 0$

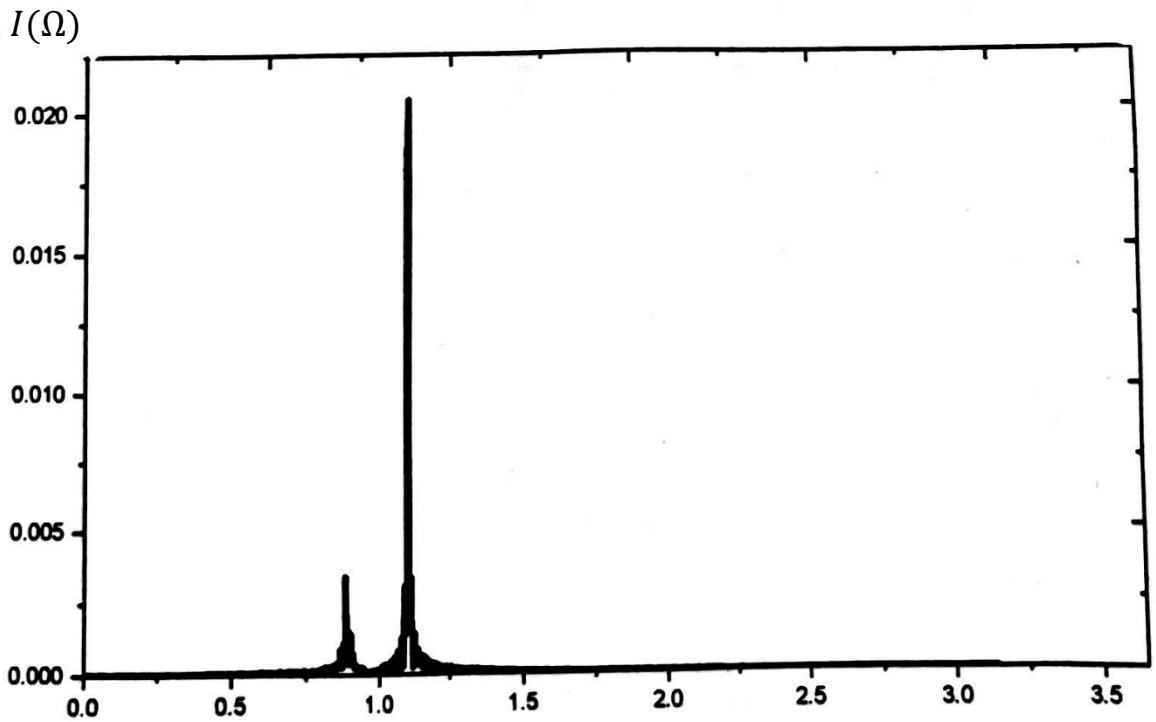

Fig. 27b

$\alpha = 0.3, \Omega = 1.1, \frac{1}{\sqrt{\beta}} = 0.04, D = 0.75$

angular velocity correlation function

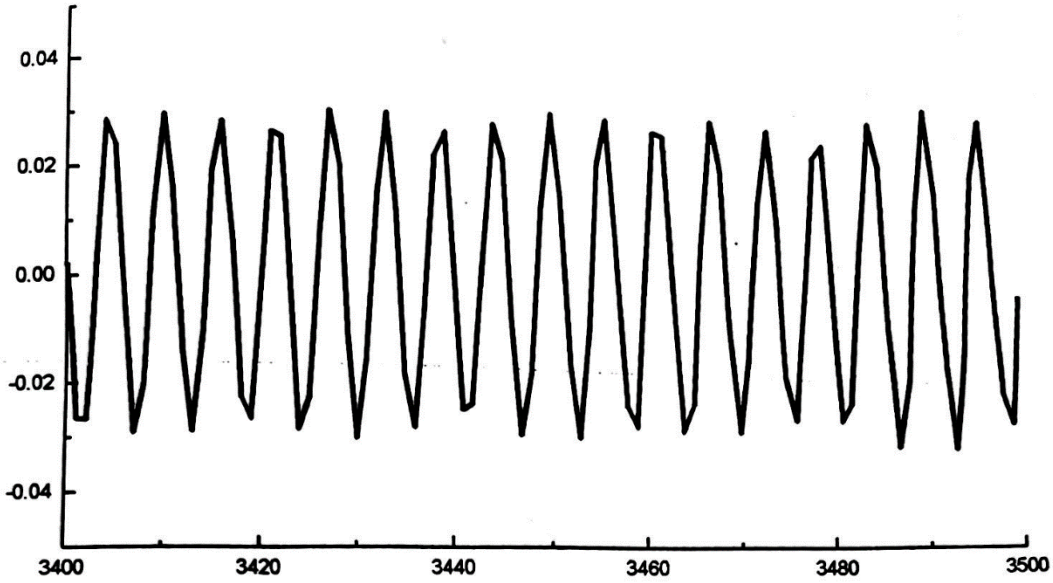

correlation time

Fig. 28

$\alpha = 0.3, \Omega = 1.1, \frac{1}{\sqrt{\beta}} = 0.04, D = 1.2$

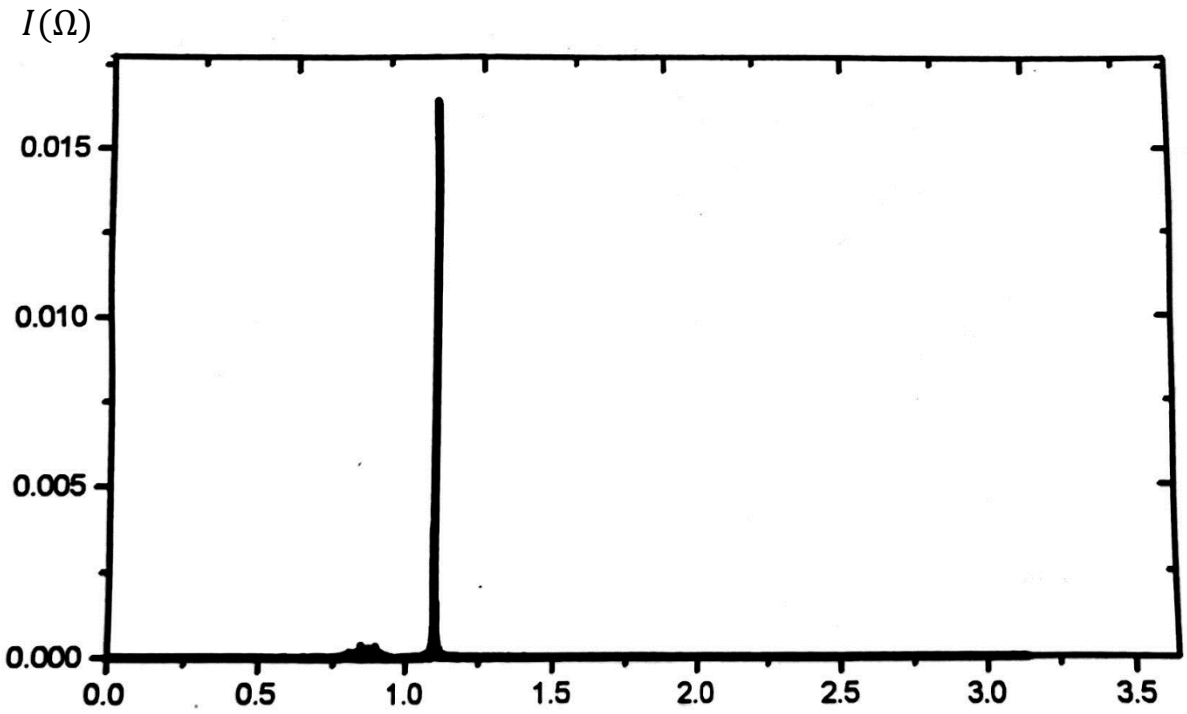

Fig. 29

$\alpha = 0.3, \Omega = 1.1, \frac{1}{\sqrt{\beta}} = 0.04, D = 1.2$

The angular velocity correlation function in Fig. 26a is again a periodic function, and there is a strong peak with the frequency of periodic torque in Fig. 27a. However, the angular velocity correlation function is an regular oscillation in both Fig. 26b and Fig. 28. Consequently, there will not be any very high peaks appear in Fig. 29. We see that peak other than the principle peak in Fig. 29 disappears. Since the angular velocity is just the time derivative of the angular position through the equation of motion. We believe that besides the appearance of very low peaks, the behavior of the power spectrum in the angular position and angular velocity cases will be almost the same.

3.2.3 SNR

When the noise is not too large, there is a peak at the frequency of external periodic torque. The amplitude $I(\Omega_0)$ rises with increasing noise strength. It reaches a maximum value corresponding to the maximum cooperation between the signal and the noise. However, this maximum value can not be a fingerprint of the stochastic resonance. Since this value may be the resonance effect of the applied external torque (noise plus periodic torque) and the natural frequency of the system. As we can not study the phenomena of stochastic resonance very clearly in the power spectrum, there is another way to describe it. The signal-to-noise ratio (*SNR*) provided an useful tool to study this effect. It is to find the critical noise strength under which an optimum cooperation occurs. Beyond this critical noise strength, the switching gradually loses coherence with the signal frequency. The dynamics then becomes noise dominated. The *SNR* is computed as: [12], [13], [14]

$$SNR = 10\log(\frac{S}{B}) \tag{3.13}$$

where *S* is the value of the output power spectrum density at Ω_0 and *B* is the value of the background at Ω_0. The unit of *SNR* is in decibels. The condition is shown in Fig. 30.

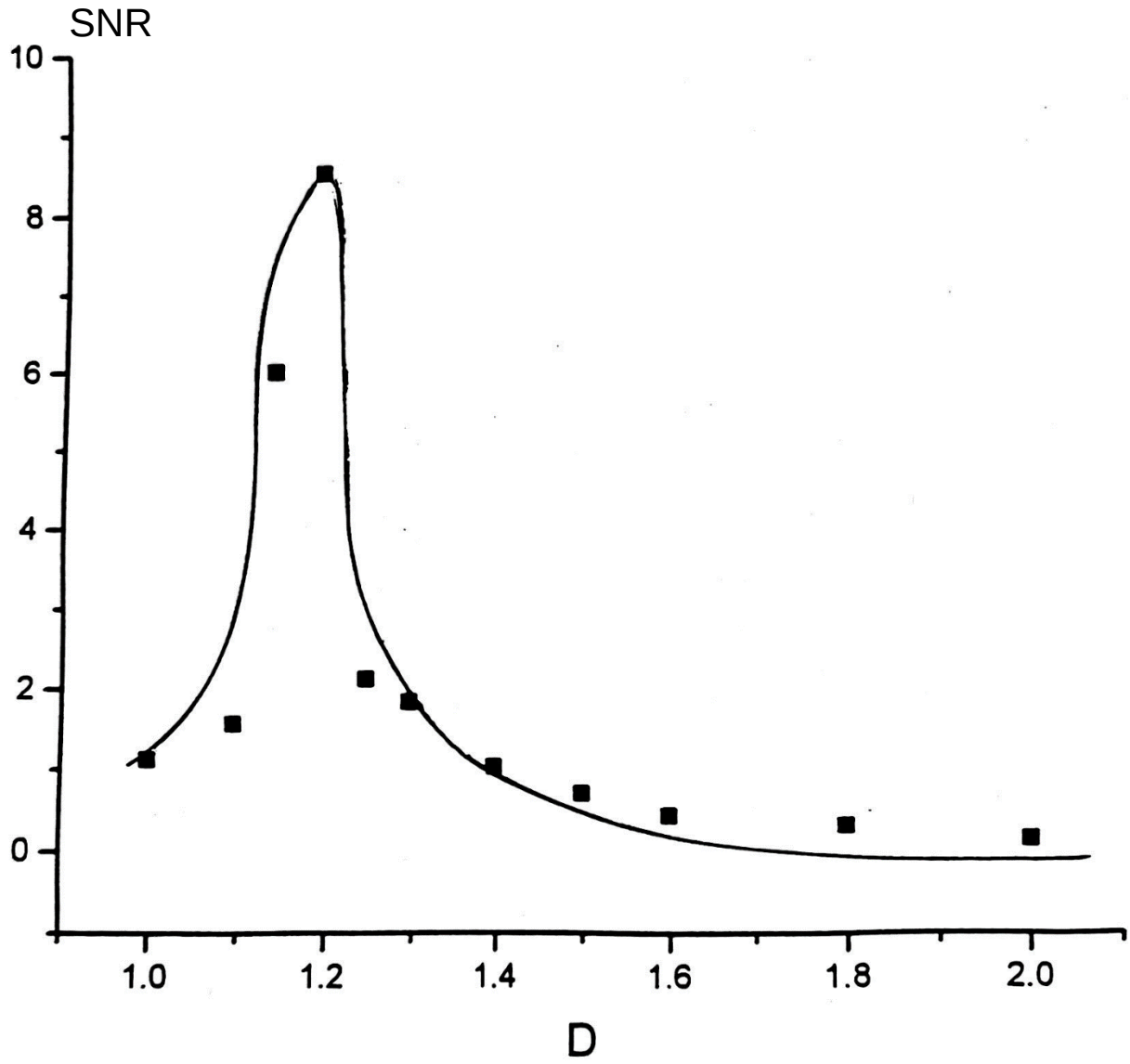

Fig. 30

$\alpha = 0.3, \Omega = 1.1, \frac{1}{\sqrt{\beta}} = 0.04$

It is interesting to see how resonance is related to the frequency of periodic torque. This situation is shown in Fig. 31a and Fig. 31b, where $\Omega_0 = 0.04, 0.2, 1.1, 2.3$ respectively.

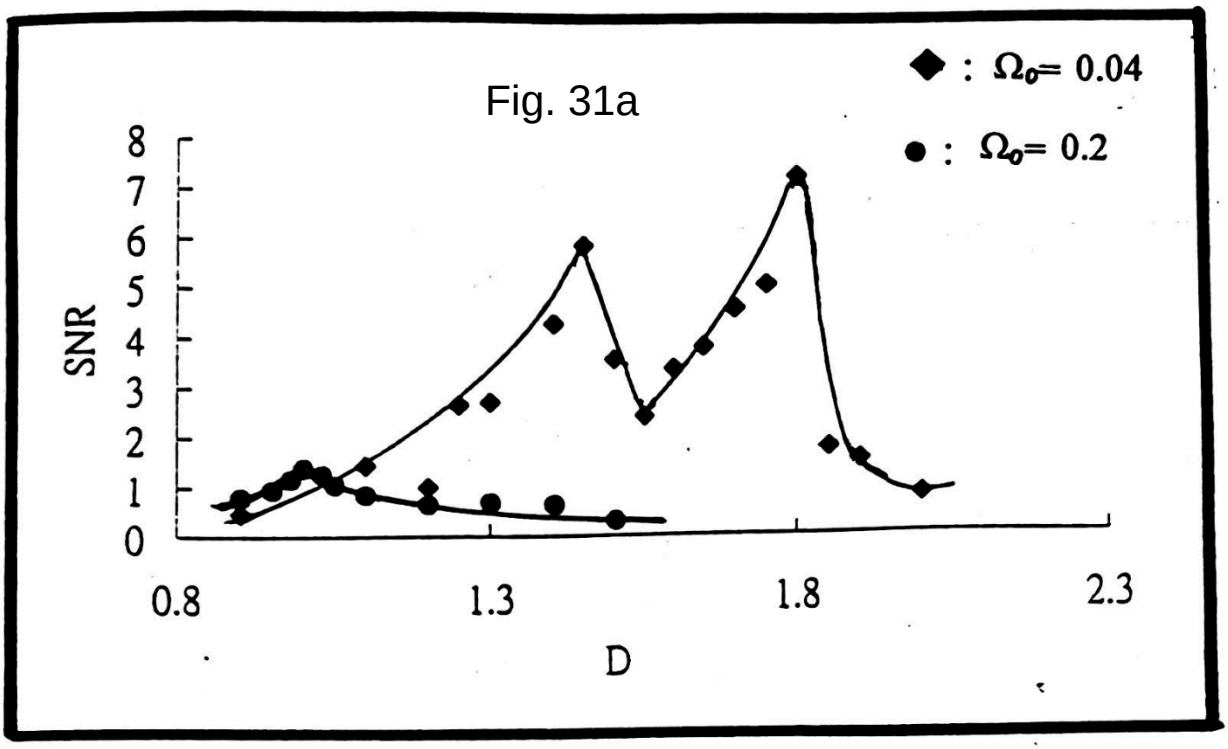

Fig. 31a

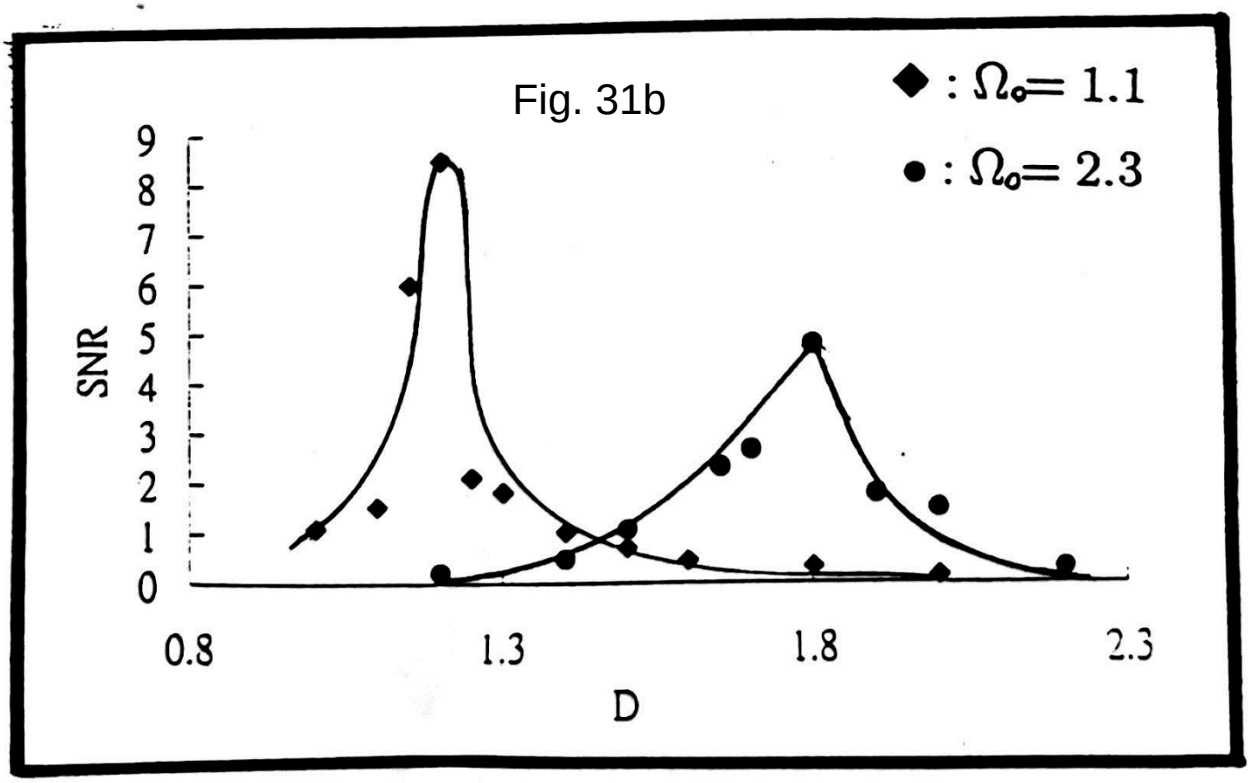

Fig. 31b

We find several interesting phenomena in Fig. 31.

1. The $\Omega_0 = 1.1$ has the largest *SNR*.

2. The peak shifts to a larger noise strength when Ω_0 increases.

3. There are two peaks for very small $\Omega_0 = 0.04$.

We first find the expression of the dependence of the absorbed energy on the periodic torque frequency. After this we can explain the above three cases. Since the damping and the strength of the periodic torque is small, the energy of the system

$$E = \frac{y^2}{2} + (1 - \cos\phi)$$

and

$$\frac{dy}{d\tau} + \frac{y}{\sqrt{\beta}} + \sin\phi = \alpha \sin\Omega\tau + \sqrt{2D}\sigma(\tau)$$

gives

$$\frac{dE}{d\tau} = y\alpha \sin\Omega\tau + \sqrt{2D}y\sigma(\tau) - \frac{y^2}{\sqrt{\beta}}$$

where the first term on the left hand side describes the energy absorption of the system out of the external torque. Let [3], [11]

$$\left(\frac{dE}{d\tau}\right)_{field} = y\alpha \sin\Omega\tau$$

$$F(\tau) = \alpha \sin\Omega\tau$$

So

$$< E_{field} > = \int_{-\infty}^{\infty} < y(\tau) > F(\tau) d\tau \tag{3.14}$$

The inverse Fourier transform of $< y(\tau) >$ and $F(\tau)$ are

$$< y(\tau) >= \frac{1}{2\pi} \int_{-\infty}^{\infty} < y(\Omega) > e^{i\Omega\tau} d\Omega$$

$$F(\tau) = \frac{1}{2\pi} \int_{-\infty}^{\infty} F(\Omega') e^{i\Omega'\tau} d\Omega' \tag{3.15}$$

Substituting (3.15) into (3.14),

$$< E_{field} >= \frac{1}{2\pi}\int_{-\infty}^{\infty} < y(\Omega) > F(-\Omega)d\Omega$$

If $\alpha \ll 1$, we can use linear response theory [11], [15] to calculate $< y(\Omega) >$, i.e.,

$$< y(\Omega) >= \psi_y(\Omega)F(\Omega)$$

where $\psi_y(\Omega)$ is the susceptibility. So

$$< E_{field} >= \frac{1}{2\pi}\int_{-\infty}^{\infty} \psi_y(\Omega)|F(\Omega)|^2 d\Omega$$

Using fluctuation-dissipation theorem

$$\psi_y(\Omega) = K_{yy}(\Omega)$$

where $K_{yy}(\Omega)$ is the Fourier transform of the angular velocity autocorrelation function, i.e.,

$$< E_{field} > \propto K_{yy}(\Omega) \qquad (3.16)$$

Hence from (3.16) the absorption of energy is related to the periodic torque frequency through the angular velocity autocorrelation function.

Here we explain (1). Consider small oscillation of the particle in the potential well without α and $\sigma(\tau)$. The potential

$$f(\phi) = -\cos\phi = f(\phi_0) + f'(\phi_0)(\phi - \phi_0) + \frac{1}{2!}f''(\phi_0)(\phi - \phi_0)^2 + \cdots$$

The oscillation frequency around the potential minimum is

$$\sqrt{f''(0)} = 1$$

So if $\Omega_0 \cong 1$, the periodic torque is in phase and resonance with the nonlinear oscillation. The particle will absorb the most effective energy. The *SNR* will be the largest.

Next we explain (2). For $\Omega_0 > 1$, we know that the absorbed energy will become smaller. However, the main effect is that the rapid variation of the period of the external torque. The transition probability will become less and it is difficult for the particle to hop to the other well during each half cycle. Increasing *D* helps by increasing the transition rate, but past the optimum *D* the increased chances will be antiphase with the external torque. This causes a gradual decline in the output signal. Thus in the high frequency regime, the maximum *SNR* will shift to a larger *D* and the *SNR* phenomena may be mostly completed by the noise other than the cooperation.

Finally we explain (3). The first peak stems from the particle which goes over the hills of the potential well. As shown in Fig. 32. It behaves as a free particle for small friction. However, this kind of dynamics is not an optimum choice for the cooperation. It is because of the running state other than the oscillation state which reflects the nature of the periodic torque and noise. As the noise increases, the behavior of the solution becomes somewhat oscillations, as shown in Fig. 33. The appearance of the second peak implies the optimum cooperation achieves. The *SNR* reaches its maximum in this situation.

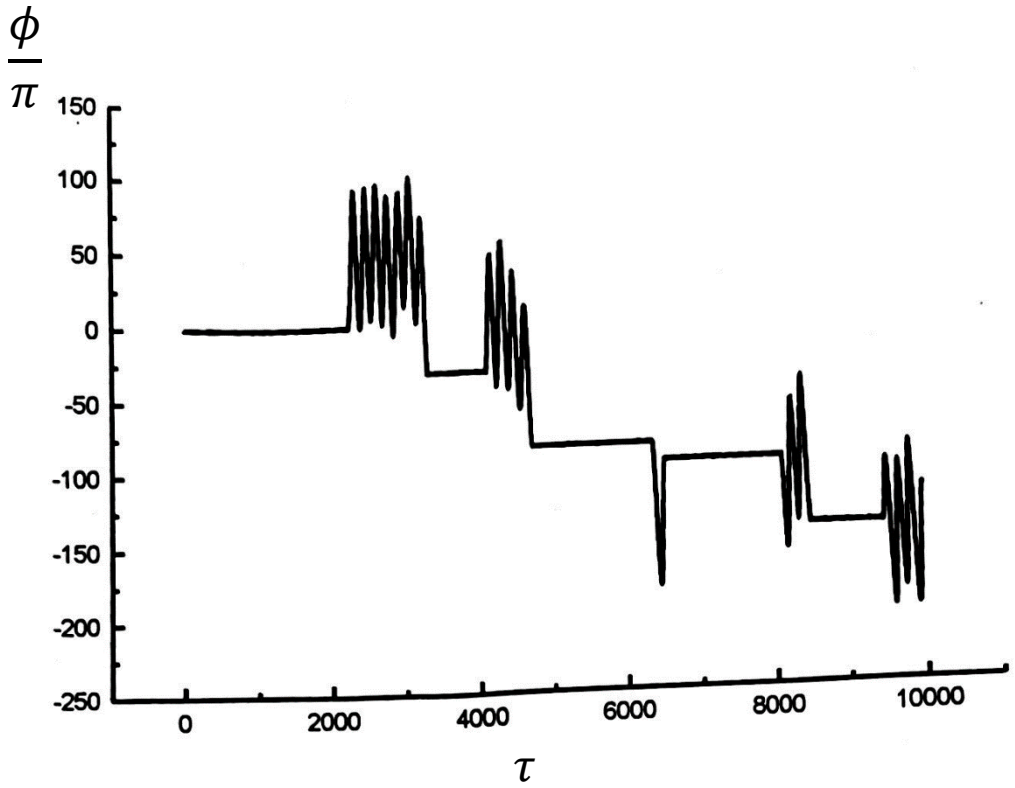

Fig. 32

$\alpha = 0.3, \Omega = 0.04, \frac{1}{\sqrt{\beta}} = 0.04, D = 1.4$

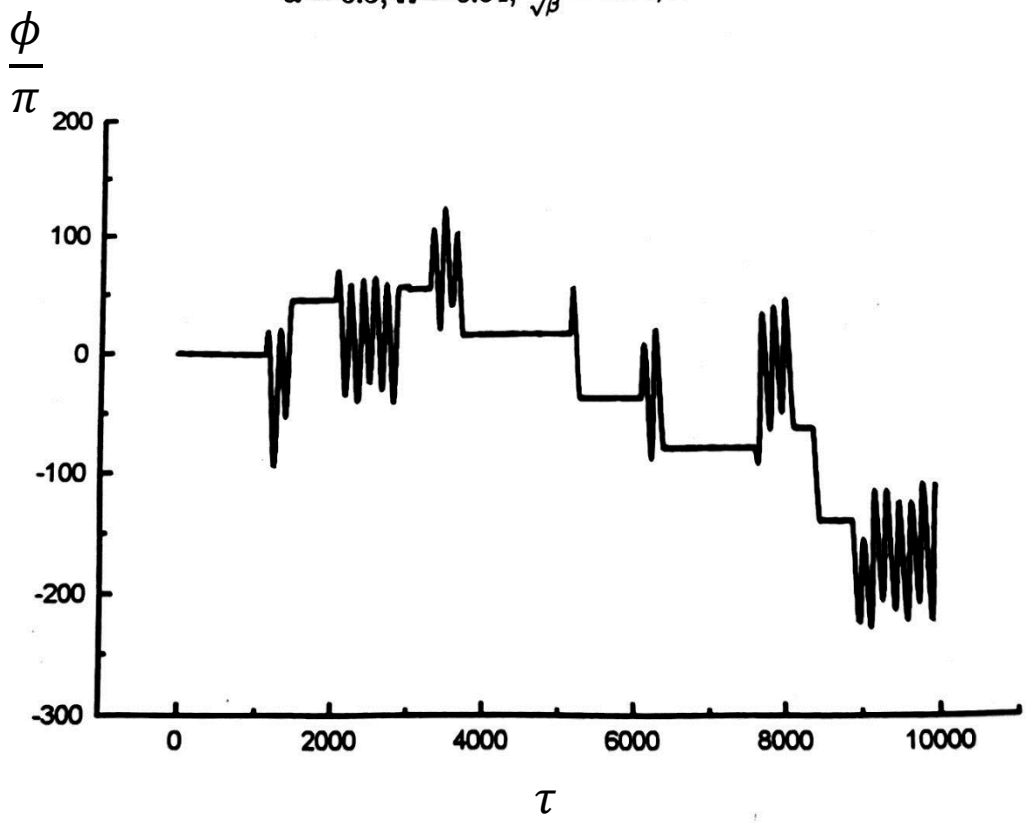

Fig. 33

$\alpha = 0.3, \Omega = 0.04, \frac{1}{\sqrt{\beta}} = 0.04, D = 1.8$

Chapter 4 Experiment explores

The experimental equipment is shown in Fig. 34.

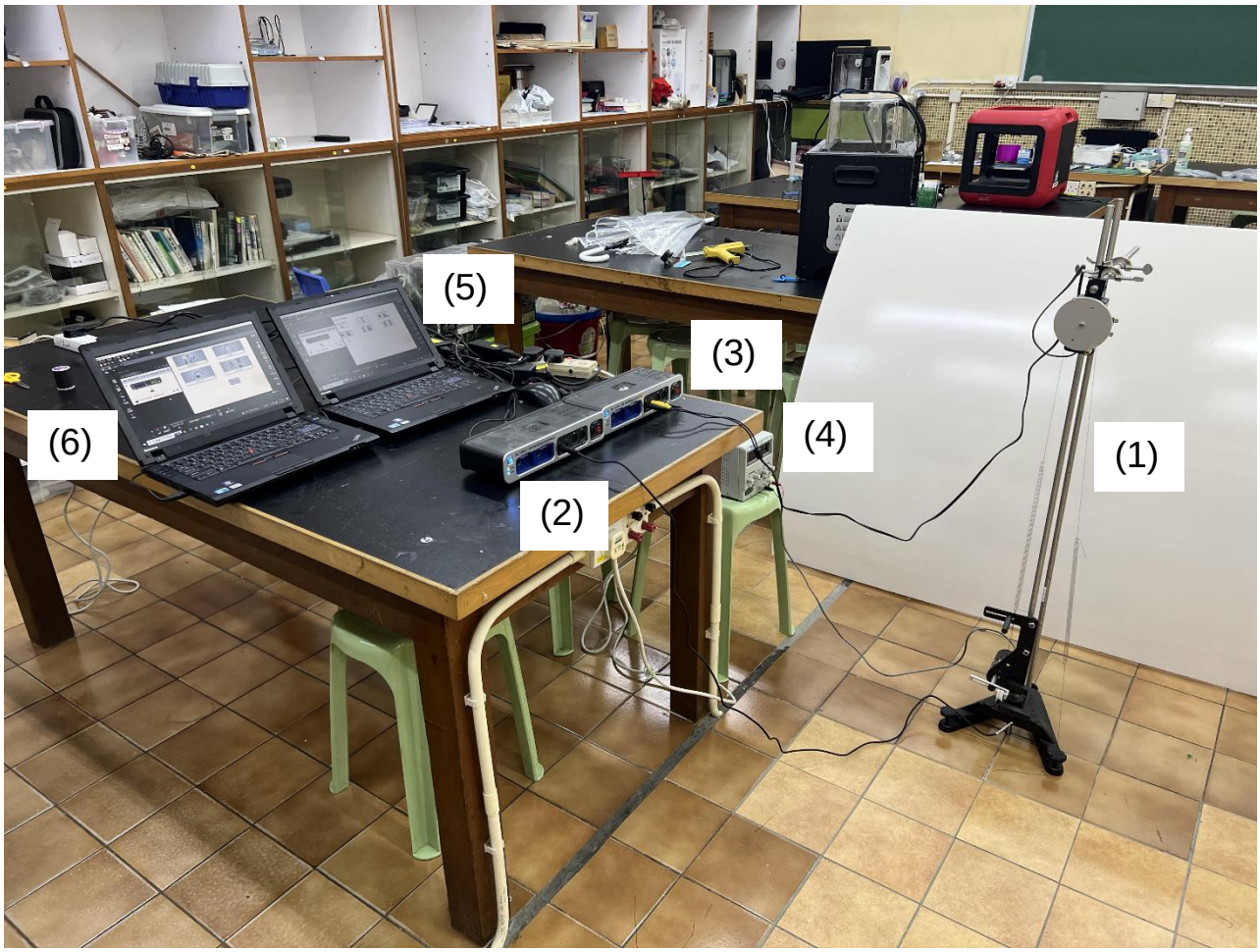

Fig. 34

The items in the figure are:

(1) The experimental system

(2) The PASCO interface connected with light gate to recorded the frequency of the external torque

(3) The PASCO interface connected with rotational motion sensor to recorded the motion of the external torque

(4) DC power supply to drive the external torque

(5) Data analysis (from light gate) in the PASCO interface

(6) Data analysis (from rotational motion sensor) in the PASCO interface

4.1 Free oscillation

We rotate the disk away from the equilibrium position and release from rest, as shown in Fig.35, the object is rotated freely under the action of gravitational torque and the resistance torque respectively.

Fig. 35

When the disk is rotating, eddy current is induced from electromagnetic induction, which generated the resistance torque on the disk. As shown in Fig. 36.

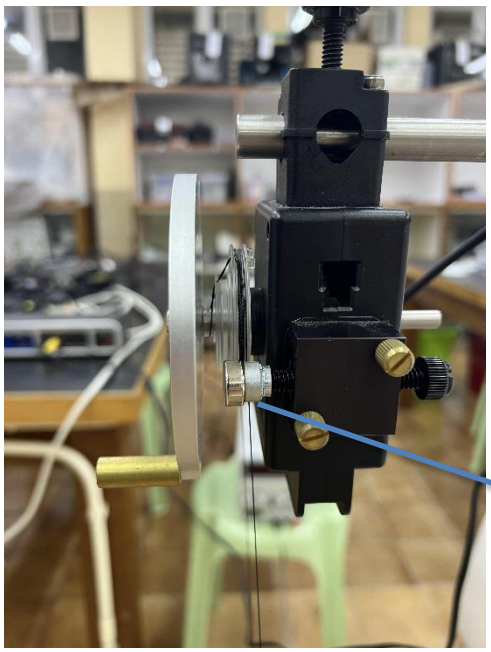

magnet which produces changing magnetic flux through the disk when it is rotating

Fig. 36

The angular displacement versus time graph and the angular velocity versus time graph are shown in Fig. 37. The motion of the disk is damped as time goes by.

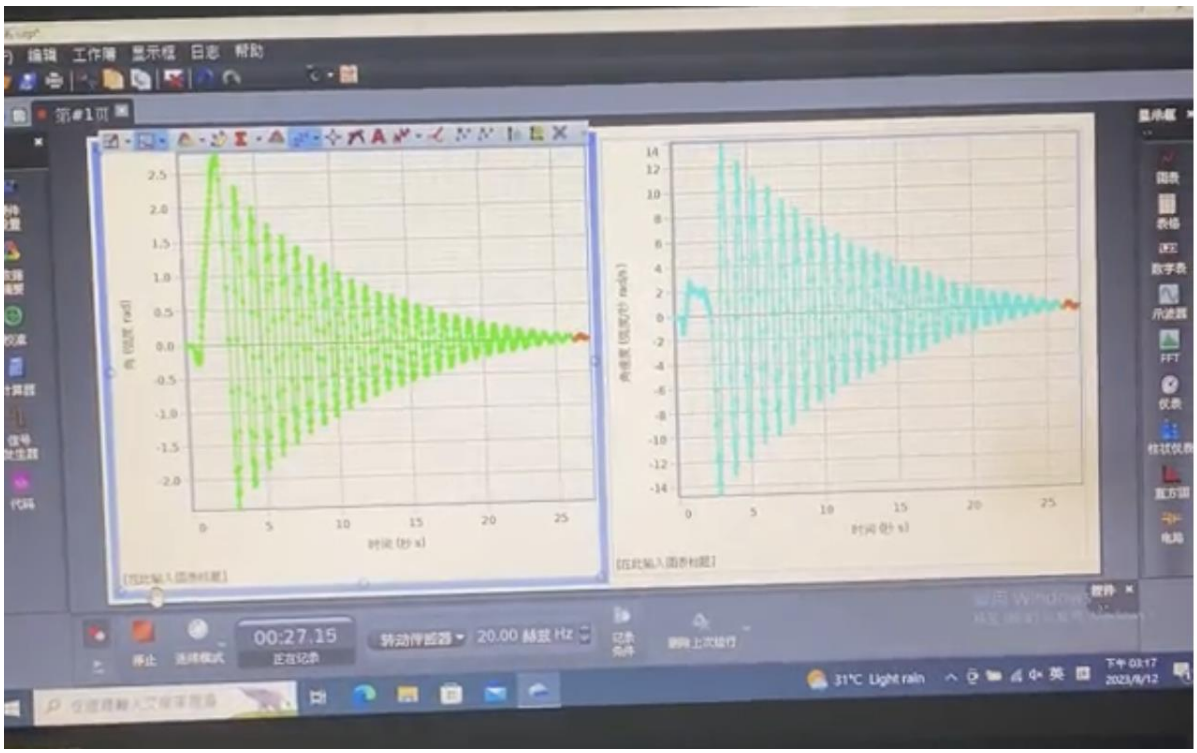

Fig. 37

4.2 Forced oscillation (constant torque)

We use four small round strong magnets to stick on another rotating disk, as shown in Fig. 38a and Fig.38b.

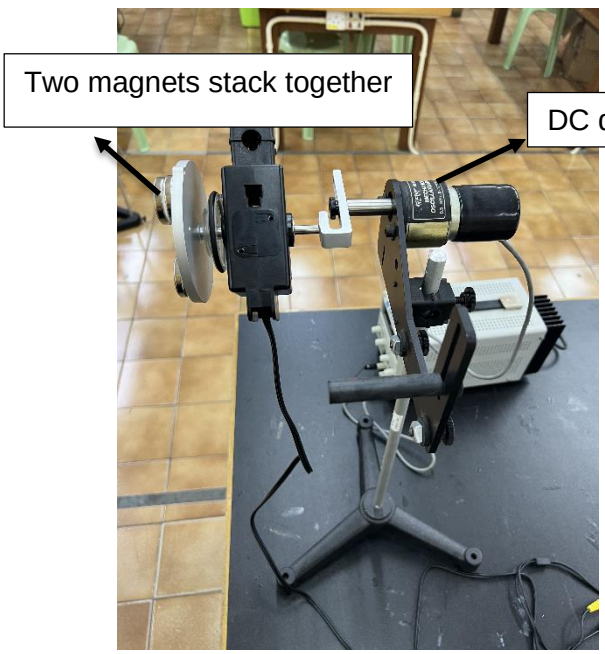

Fig. 38a

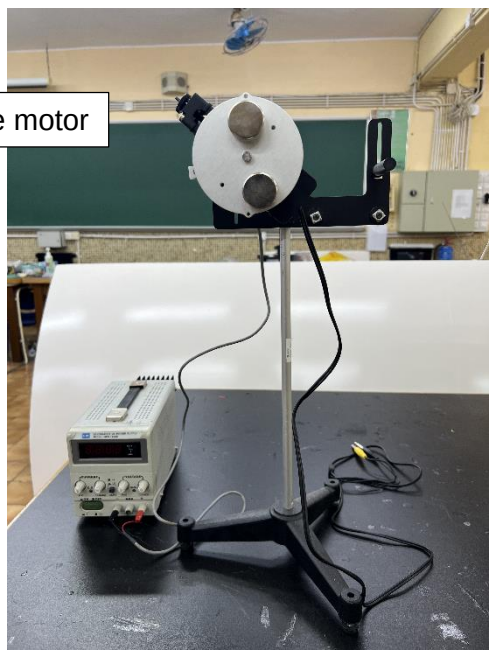

Fig. 38b

When the rotating disk is close to the stationary disk mounted on the system, as shown in Fig. 39a, due to the effect of electromagnetic induction, induced current is generated on the surface of the disk. Under the action of periodic changing external magnetic field, an induced magnetic moment will be generated on the disk. When the rotating disk rotates in a specific direction, a torque in the same direction as the rotational disk will act on the stationary disk at the same time. As long as the distance between the two disks remains constant and by keeping the rotational speed of the rotating disc constant, an external constant torque can be generated on the disk of the system.

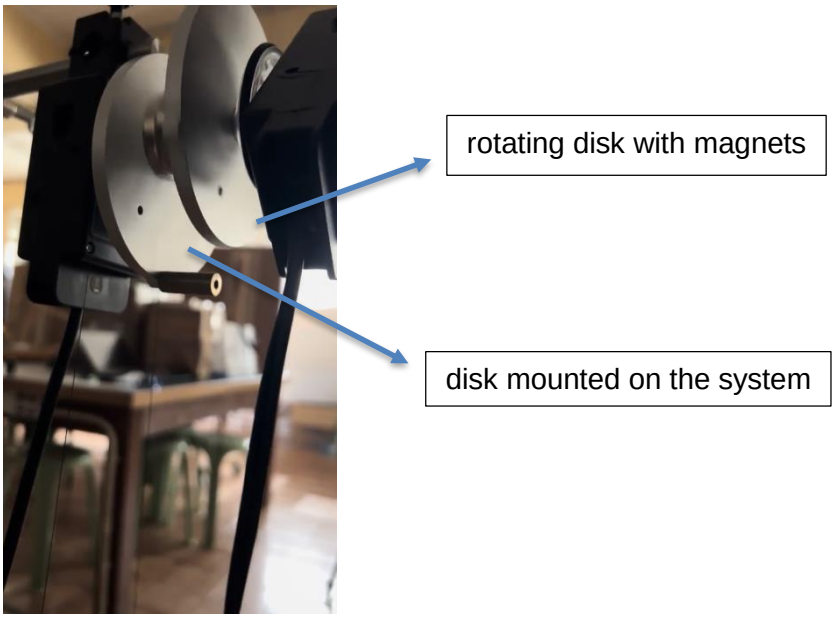

Fig. 39a

The phase diagram of the disk is shown in Fig. 39b. There is a limit cycle with small amplitude in the phase diagram.

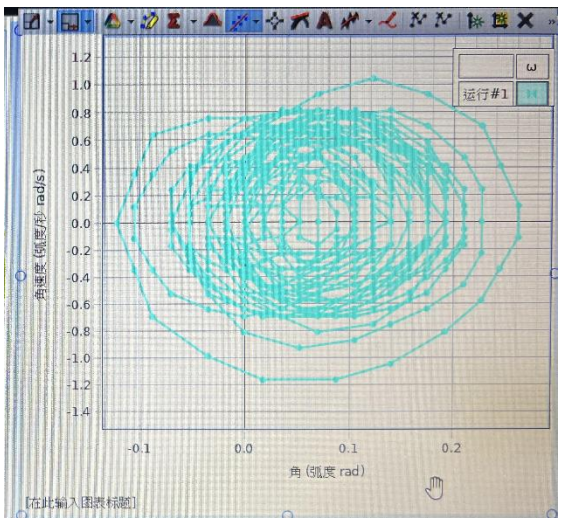

Fig. 39b

4.3 Forced oscillation (periodic torque)

We use a DC motor to generate a periodic torque, as shown in Fig. 40a, which acted on the system. The greater the input voltage, the higher the motor speed and the greater the frequency of the torque. Hence we increase the voltage, the disk rotates more rapidly. The amplitude of the torque can be determined by changing the length of the moment arm connected to the rotating shaft, as shown in Fig. 40b. The longer the moment arm is, the larger the torque amplitude will be. By adjusting the value of the voltage and the length of the arm, the magnitude and frequency of the periodic torque can be changed. Using the data measured by the rotatory motion sensor installed on the disk, the relationship between the angular displacement and the angular velocity of the disk can be measured over time.

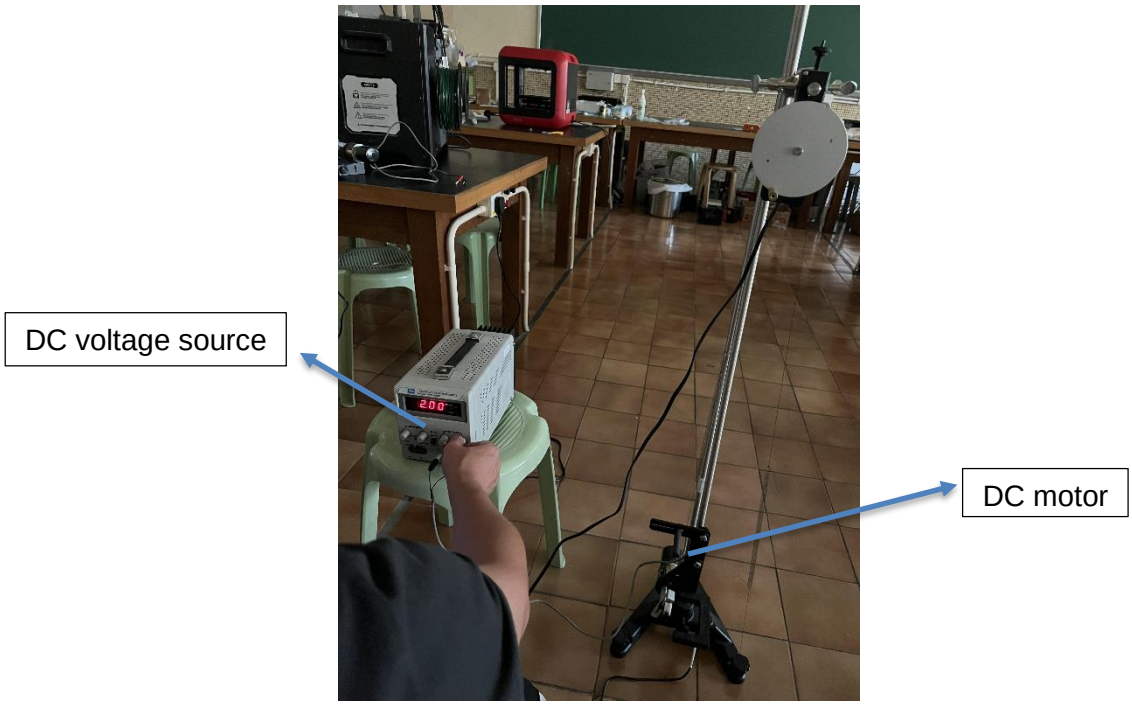

Fig. 40a

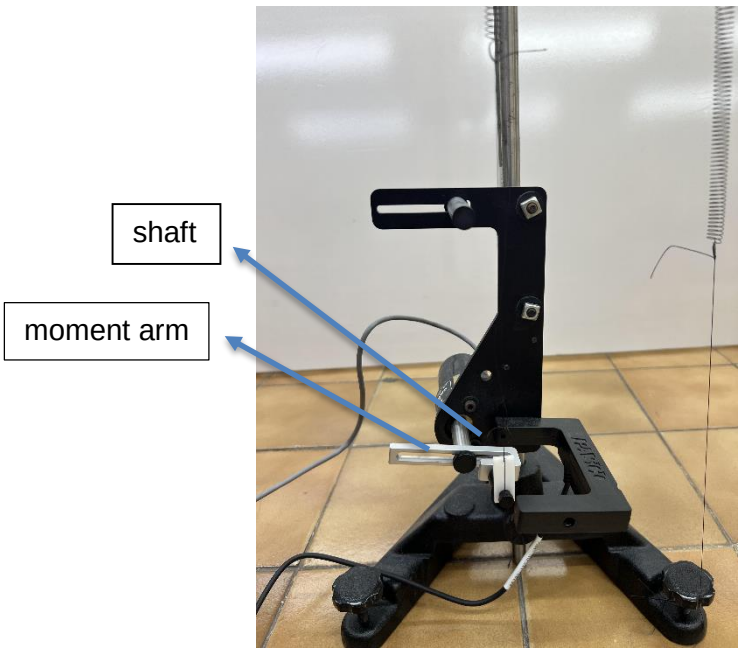

Fig. 40b

The phase diagram of the disk is shown in Fig. 40c. After a transition time, the rotation of the disk tends to several limit circles with the same center. It can be judged that the rotation mode of the disk is composed of several periodic motions of different frequencies under the action of a single-frequency periodic torque. It is a characteristic nature of nonlinear rotation, that is, when a certain frequency is input into the system, the output of the system includes several frequencies, i.e., the motion of the disk is composed of several subharmonic modes.

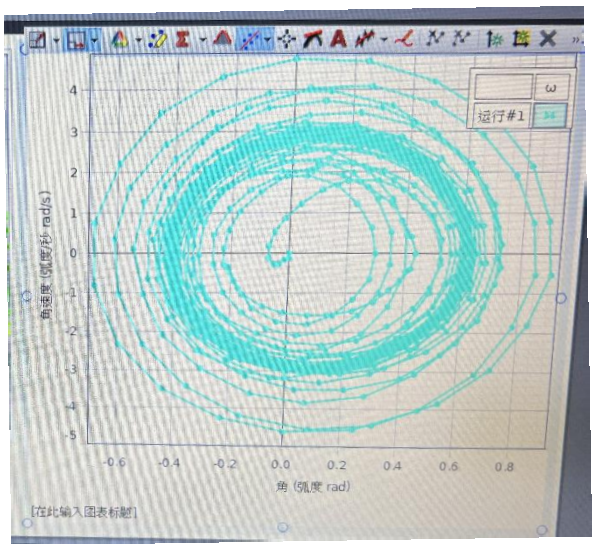

Fig. 40c

4.4 Forced oscillation (periodic torque and random torque)

To generate random torque, we use the following method:

1. Use the Arduino control board to load the Arduino program that can generate random signals.
2. Connect the motor driver circuit board to the Arduino control board.
3. Connect the DC voltage to the motor drive circuit board.
4. Connect the DC motor to the motor drive circuit board, as shown in Fig. 41a.
5. Connect the DC motor to one end of the spring mounted on the system, and connect a motor capable of generating periodic torque to the same end of the same spring, as shown in Fig. 41b.

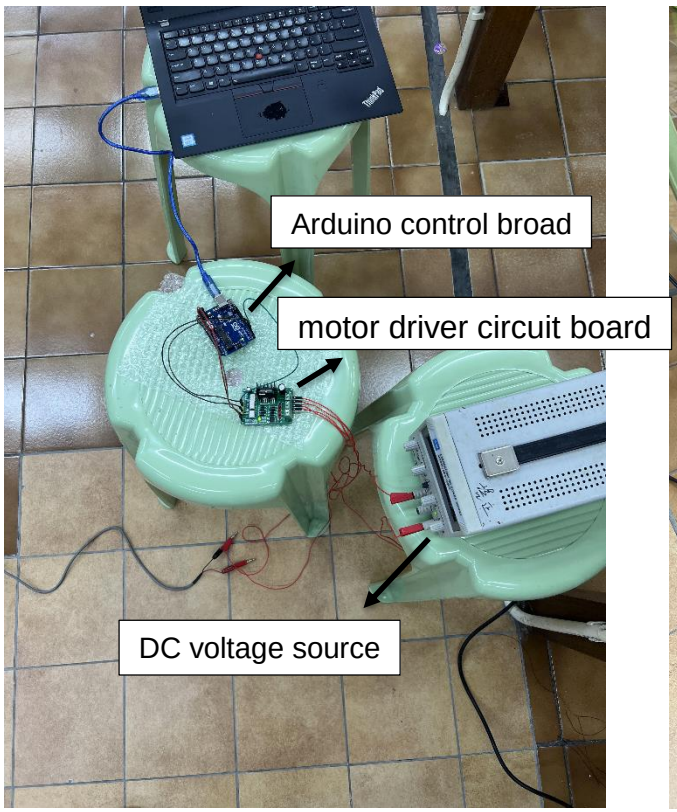

Fig. 41a

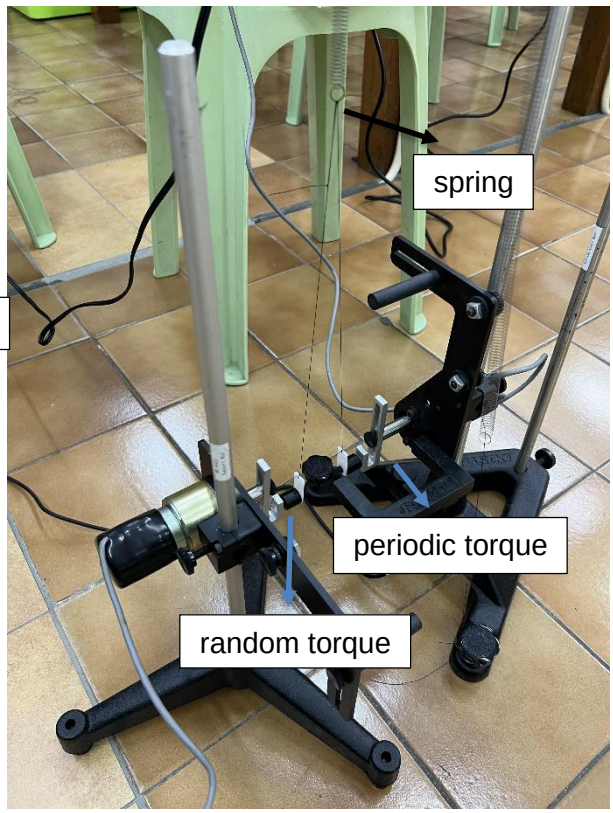

Fig. 41b

When the power is turned on, the Arduino control board transmits the program to the motor drive circuit board. When the circuit board receives the program, it will input a DC voltage signal of random intensity to the motor, i.e., the motor will be driven by random voltage. The random rotation of the motor inputs random torque to the disk in the system. When two DC motors are started at the same time, both the periodic torque and random torque will act on the disk of the system at the same time. Under the simultaneous action of these two torques, the disk will exhibit specific periodic motion.

The phase diagram of the rotating disk is shown in Fig. 41c, the limit cycle is complex and also composed of several subharmonic with different frequencies and different amplitudes.

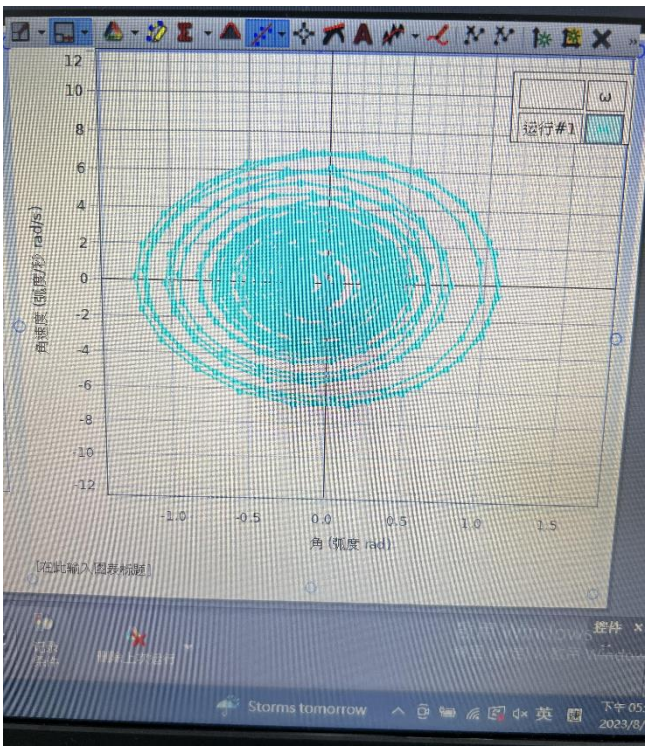

Fig. 41c

Chapter 5 Conclusions

We had studied the dynamics of the complex pendulum system by nonlinear method. The pendulum behavior in the noiseless case can be divided into two parts:

1. Autonomous case: The system undergoes two different behaviors. They are separated by a bifurcation curve. The appearance of fixed points in the system described the first kind of motion. There are two kinds of fixed points in this system. When the dynamics stops at $\phi^* = \sin^{-1}\rho$, the fixed point is a sink. Furthermore, if $\frac{1}{\sqrt{\beta}} - 4\cos\phi^* > 0$, it is a stable node. If $\frac{1}{\sqrt{\beta}} - 4\cos\phi^* < 0$, it is a stable spiral. When it stops at $\phi^* = \pi - \sin^{-1}\rho$, the fixed point is a saddle. We calculate the bifurcation through Melnikov's method. Here we consider the damping and the constant torque are perturbation to the original Hamiltonian system. When $\rho < 1$, the bifurcation occurs at $\rho = \rho_c = \frac{4}{\pi\sqrt{\beta}}$. This is a homoclinic bifurcation, i.e., some part of a limit cycle (running solution) moves closer to the saddle point and becomes a homoclinic orbit eventually. This phenomena is an hysteresis effect. However, when $\rho_c > 1$, there will not has such effect. When $\rho = 1$, there occurs a saddle-node bifurcation. All orbits join to an unique running solution. This gives non-zero angular velocity in the motion. The relationship between the constant torque and angular velocity is one to one. The pendulum will jump discontinuously to a zero angular velocity state when ρ decreased to $\frac{4}{\pi\sqrt{\beta}}$. The period of the limit cycle will tend to infinity at the homoclinic bifurcation.
2. Nonautonomous case: The system behavior at $\rho < 1$ will be more complex because of the external periodic torque. There are several bifurcation curves governed the system behavior when $\rho < 1$. Instead of the fixed points, there are some limit cycles (oscillating solutions) which attract the nearly orbits. They become more unstable as ρ exceeds every bifurcation curve. When $\rho > \rho_c^+$, some initial conditions lead to a running solution. This is the hysteresis effect. As $\rho > 1 - \alpha$, all solutions are running solutions and $\rho = 1 - \alpha$ is the maximum zero angular velocity torque. When Ω is very small, the attracting limit cycle becomes smaller, i.e., there is a resonance region for which the system will absorb most energy from the periodic torque. When Ω is very large, we use average theorem to calculate the

bifurcation curves. We find this curves are almost the same as in the autonomous case. The most striking effect of periodic torque on the pendulum is the appearance of steps. This steps reflect the periodicity of the running solutions. We had proved that not all periodic running solutions gives the steps. Besides steps, the system behavior in the non-zero angular velocity case will have the linear relationship. And there will be no hysteresis effect for heavy damping case.

We also add a white noise term to the system. The behavior will be very different depends on the value of noise.

1. When the noise is very small, we use perturbation to calculate the angular position autocorrelation function. We also stimulated the power spectrum of the angular position and the angular velocity. The noise will enlarge peaks. The strength of the low frequency peaks in the angular velocity case become weaker. It is because of the strength of such peaks are multiplied by the correspond Ω with respect to the angular position case.
2. When the noise is large, there will be some escape events take place in the system. It is because of the cooperation of noise and the periodic torque. This is called Stochastic Resonance. It only occurs in nonlinear systems. We study this phenomena through the power spectrum analysis. There always exists a peak at the same frequency as the periodic torque. The noise power spectrum has a Lorentzian-like shape. The ultra-low frequency peaks represented the long periodicity of the angular position autocorrelation function. At the same time, the angular velocity autocorrelation is a regular oscillations. The optimum cooperation can be studied through *SNR*. We find the *SNR* peak shifts to a larger *D* as Ω_0 increases. The peak strength is related to the absorbed energy from the periodic torque. However, there may not be only one peak in the *SNR* for every Ω_0. This reflects the multiwell nature of the nonlinear complex pendulum system.

References

1. J. Guckenheimer, P. Holmes, Nonlinear Oscillations, Dynamical System, and Bifurcations of Vector Fields, Spring-Verlag, New York, Chap. 4 (1993)
2. C. D. Hu, Phys. Rev. B (54), 10065-10073 (1996)
3. H. Strogatz, Nonlinear Dynamics and Chaos, Addison Wesley, Chap. 8 (1996)
4. D. W. Jordan and P. Smith, Nonlinear Ordinary Differential Equations, Clarendon Press· Oxford, (1998)
5. V. A. Pliss, Nonlocal Problems of the theory of Oscillations, Academic, New York, Chap. 2 (1996)
6. P. Coullet, J. M. Gilli, M. Monticelli, N. Vandenberghe, A damped pendulum forced with a constant torque, American Journal of Physics (2005)
7. Arfken, Weber, Mathematical methods For Physicists, 4th ed., Academic, Chap. 17 (1995)
8. Aline Souza de Paula, Marcelo Amorim Savi, Wallace Moreira Bessa, Chaos Control in a nonlinear pendulum through an adaptive fuzzy sliding model based approach, 19th International Congress of Mechanical Engineering (2007)
9. Aline Souza de Paula, Marcelo Amorim Savi, Francisco Heitor Iunes Pereira Pinto, Complex behavior of an experimental nonlinear pendulum: Chaos and transient chaos, 18th International Congress of Mechanical Engineering (2005)
10. Robert DeSerio, Chaotic pendulum: The complete attractor, Am. J. Phys. 71 (3), (2003)
11. M. Toda, R. Kubo, N. Hashitsume, Statistical Physics 2, 2nd ed., Springer, New York, Chap. 1, 2 (1995)
12. Adi R. Bulsara and Luca Gammaitoni, Physics Today, 39, March (1996)
13. Luca Gammaitoni, Peter Hanggi, Peter Jung, Fabio Marchesoni, Stochastic resonance, Reviews of Modern Physics, Vol. 70, No. 1, January (1998)
14. Shan Yang, Zening Fan, Ruibin Ren, The Stochastic Resonance Phenomenon of Different Noises in Underdamped Bistable System, Advanced in Mathematical Physics, (2021)
15. H. Risken, The Fokker-Planck equation, Springer- Verlag, Berlin (1989)